SISSA - SCUOLA INTERNAZIONALE SUPERIORE STUDI AVANZATI
TRIESTE
Strada Costiera 11

ISAS - INTERNATIONAL SCHOOL FOR ADVANCED STUDIES

Thesis submitted for the degree of
"Doctor Philosophiae"

First-Principle Molecular Dynamics Simulations of Disordered GaAs

CANDIDATE
ZHANG Qiming

SUPERVISORS
Prof. A. Selloni
Prof. R. Car
Prof. M. Parrinello

Academic Year 1988/89

TRIESTE

ACKNOWLEDGEMENTS

This work has been carried out under the supervision of Profs. Annabella Selloni, Roberto Car and Michele Parrinello. I am deeply grateful to them for their patient guidance and kind encouragement. Special thanks are due to Prof. Annabella Selloni for her careful reading of the manuscript. I would like express my thanks to Dr. Guido Chiarotti for his help on programming and beneficial discussions. I thank Prof. Stefano Baroni who kindly made his computer code for crystalline GaAs available to me. I am also grateful to Dr. Kurt Ding who gave his good suggestions on the thesis writing.

This work has been in part supported by the SISSA-CINECA (Centro di Calcolo Elettronico dell'Italia Nord-Orientale) collaborative project, under the sponsorship of the Italian Ministry for Public Education.

Contents

1 Introduction 1

2 Car-Parrinello Method 5

2.1 Classical Molecular Dynamics 5

2.2 Adiabatic Approximation 8

2.3 Electronic Ground State at a Fixed Ionic Configuration 9

2.4 *ab-initio* Molecular Dynamics 11

3 Technical Aspects: Pseudopotentials for Ga and As and the Kleinman-Bylander Scheme 15

3.1 General Discussion 15

3.2 Testing the KB scheme for c-GaAs 20

3.3 Using the KB scheme for *ab-initio* molecular dynamics . 24

4 Liquid GaAs 26

4.1 Technical Details 26

4.2 Structural Properties 28

4.3 Dynamical Properties 35

4.4 Bonding 38

4.5 Electronic Properties 44

5 Simulated Quenching of GaAs 49

6 Conclusion 56

A The Nosè Thermostat 58

bibliography 62

Chapter 1

Introduction

The properties of gallium arsenide (GaAs) have been the subject of intensive study for over 20 years due to its fundamental and technological interest. At room temperature, GaAs is a compound semiconductor combining group *III* and group *V* elements from the same row in the periodic table as the archetypal group *IV* semiconductor, germanium. Crystalline GaAs(c-GaAs) has a zinc blende structure which consists of two interpenetrating face-centred cubic lattices containing Ga and As atoms respectively. Atoms thus arrange themselves in chemical order, *i.e.* one atom bonds with four unlike-atoms. Similarly to silicon and germanium, which have diamond structure, the bond angle in the c-GaAs is 109°, giving a locally tetrahedral structure. What is significantly different from silicon and germanium is a valence charge shift from Ga to As atoms, adding an ionic component to the predominantly covalent bond. This has very important effects on the electronic band structure. For instance, the wider band gap, among others, maintains device performance to higher temperature, whereas the larger curvature at the bottom of the conduction band gives a lighter effective mass

($m^* \propto [d^2E/dk^2]^{-1}$) and hence high electron mobility. It is well known that the electronic properties of semiconductors can be changed dramatically by doping. In Si and Ge, impurity atoms from groups *III* and *V* can substitute host atoms to produce shallow donors and acceptors in the material. In c-GaAs, because substitutional impurity atoms from groups *II*, *IV* and *VI* can act as shallow donors and acceptors, extra degrees of freedom are available when compared to the situations in Si and Ge. In summary, GaAs is a material of great interest, both from a fundamental point of view, as a prototype compound semiconductor, and for technological applications, such as the formation of lattice-matched heterojunction (and/or superlattice) structures with, *e.g.* GaAlAs.

Studies of disordered semiconductors have become more and more active recently. A major part of this activity is concerned with the solid, *i.e.* amorphous phase, but the liquid has also received increasing attention both for its fundamental interest and because of its relevance to technologically important processes such as crystal growth from the melt. Although most experimental and theoretical efforts so far have focused on the disordered phases of the elemental semiconductors, particularly Si and Ge, the disordered compound semiconductors are of much potential interest, because they offer the possibility of investigating, among others, how the mixed(covalent/ionic) bonding between the two constituent atomic species affects the structure and hence the electronic properties of the material. In compound disordered semiconductors, for example, chemical defects such as "wrong"(or like-atom) bonds –which are absent in elemental semiconductors as well as in the perfect crystalline phase of such materials–emerge with a relatively large probability, particularly in the liquid phase. These defects are expected

to have a considerable influence on optical and electronic properties.

Experiments show that similar to Si and Ge, GaAs becomes metallic and increases its density upon melting [1]. Neutron diffraction results indicate that the larger density of the liquid phase is related to a variation of the coordination number, from the value 4 typical of the crystal to a value of approximately 5.5($\pm$0.5), while a slight increase of the average interatomic separation takes place [2]. Amorphous (a-) GaAs, instead, is still a semiconductor and exhibits short range tetrahedral order as a-Si and a-Ge, with a coordination number of $\sim$4 and a bond angle of $\sim$ 109°[3]. In a-GaAs, there are not only structural defects related to the occurrence of "dangling bonds"(*i.e.* broken bonds) like in a-Si and a-Ge, but also chemical defects consisting in "wrong bonds". These defects strongly depend on the process of preparation of the amorphous materials.

Theoretically, because of the lack of periodicity, symmetry and long range order in a disordered system, there is no simple formalism that can be used in the calculation of its microscopic properties, as those used to study crystals. The small number of available experiments, such as a diffraction or EXAFS, usually give only the radial distribution function, from which the generation of the underlying three-dimensional structure is not unique. Understanding the microscopic structure of disordered semiconductors and its influence on the electronic properties is an attractive and difficult task. One way is the construction of models. Unfortunately, no acceptable model for liquid semiconductors has been reported so far. For the amorphous phase, a widely used model is the so-called "continuous random network"(CRN)[4], which constructs a random network by connecting a number of tetrahedra with some

degree of bond-angle distortion and more or less complete freedom for values of the dihedral angle. However, defects such as dangling bonds or "wrong bonds" which are important to the electronic properties are hardly included in these models, and a possible bias may be introduced into the network by the model builder. More systematic approaches to the description of disordered systems are molecular dynamics(MD) or Monte Carlo techniques. However, the application of these schemes to semiconductors is largely limited by our knowledge of the interatomic interactions in these materials (to be discussed in chapter 2). These limitations are overcome in a first-principle MD scheme proposed recently by Car and Parrinello [5]. Its success has been witnessed in numerous studies of the liquid [6] [7] and amorphous phases [8] [9] of some elemental materials, *e.g.* Si, C, Se *etc.*. The noticeable feature of this scheme is that the interatomic potential is constructed directly from the electronic ground state calculated by density-functional formalism.

In this thesis, this first-principle MD, to be introduced in chapter 2, is applied for the first time to the study of a compound system—GaAs. A careful test of the pseudopotentials used for Ga and As is given in chapter 3. In chapter 4, we present our simulation of liquid GaAs at a temperature near the melting point. Both the atomic and electronic properties are obtained, which are in good agreement with available experimental data. A few results on a-GaAs are presented in chapter 5. In chapter 6, we give our conclusions.

Chapter 2

Car-Parrinello Method

2.1 Classical Molecular Dynamics

The basic ingredient of a molecular dynamics(MD) simulation is to compute trajectories of a system and to perform time averages along the computed trajectories. By the ergodic hypothesis, such time averages are then treated as the thermodynamic ensemble averages for equilibrium systems. The implementation of the classical MD is straightforward. For a system of N classical particles with the interaction potential $\Phi(\vec{R}_1, \ldots, \vec{R}_N)$, the trajectories, i.e. the coordinates $\vec{R}_I(t)$ and velocities $\dot{\vec{R}}_I(t)$ at time t, $(I = 1, \ldots, N)$, can be obtained through a numerical integration of Newton's equations

$$M_I \ddot{\vec{R}}_I = -\nabla_{\vec{R}_I} \Phi(\vec{R}_1, \ldots, \vec{R}_N), \quad I = 1, \ldots, N \tag{2.1}$$

where the dots indicate time derivatives, and M_I is the mass of the I-th particle. For practical reasons, the number of particles, N, is chosen to be finite. To simulate a bulk system, periodic boundary conditions are therefore used to eliminate surface effects.

In the classical MD, the major input are the interatomic interactions that govern the motions of atoms. The application of MD to a real system is largely limited by our knowledge of the interaction potential $\Phi(\vec{R}_1, \ldots, \vec{R}_N)$ among the particles. Generally speaking, a potential describing interactions among N particles can be resolved into one-, two-, three-, *etc.*, up to N-body contributions,

$$\Phi(\vec{R}_1, \ldots, \vec{R}_N) = \sum_I v_1(\vec{R}_I) + \sum_{I<J} v_2(\vec{R}_I, \vec{R}_J) + \sum_{I<J<K} v_3(\vec{R}_I, \vec{R}_J, \vec{R}_K) + \ldots + v_N(\vec{R}_1, \ldots, \vec{R}_N) \tag{2.2}$$

In practice, to perform a simulation, it is necessary that the component functions v_n converge quickly to zero with increasing n. Traditionally, simple two-body potentials such as the hard sphere or the Lennard-Jones potential have been used to perform MD simulations and reasonably good results have been obtained for simple systems such as noble gases[10]. More elaborate effective pair potentials have been used quite successfully to describe some simple metals[11]. However two-body potentials (pair interactions) can hardly give a good description of a large group of systems including semiconductors[12].

The one-body term is normally contributed by external fields. Its main role, in most cases, is to affect the thermodynamics of a system. The structural aspect, on the other hand, is largely determined by the higher order terms. The expansion including one- and two-body terms is therefore the simplest approximation. As already pointed out, its application is unfortunately limited to a rather small number of simple systems. For systems of increasing complication, higher order terms, say, three- and even four-body terms, are needed. For example, a number of empirical interatomic potentials including three-body contributions have

been proposed for Si, as no reasonably good pair potentials succeeded in stabilizing its characteristic tetrahedral structure. In spite of some progress, none of these models can describe satisfactorily the structural properties of the various phases of Si[13]. Furthermore, the information about electronic properties is missing completely in these classical MD simulations. This is, perhaps, the most serious defect of the classical MD simulation.

On the other hand, much progress has been made during the past few decades in the first-principle calculation of various properties of crystalline solids by using density-functional(DF) theory[14]. The local density approximation (LDA)[15] has been successfully applied to calculate the static and dynamic structures of c-Si and c-Ge, the relative stability of different phases, and their pressure-induced phase transformation[16]. Also, the valence charge density computed from LDA is in satisfactory agreement with experiment. However, these computations often involve many iterations to reach self-consistency. Furthermore, such a computational complexity makes it difficult to apply the LDA to investigate disordered systems.

Recently, Car and Parrinello[5] have proposed an efficient scheme which combines DF theory with MD simulations. Their scheme allows for an equal treatment of electrons and ions, in a self-consistent way under the Born-Oppenheimer approximation. In such an *ab-initio* MD simulation, the interatomic forces are derived directly from the electronic ground state, calculated using the LDA.

2.2 Adiabatic Approximation

Real materials consist of an enormous number of electrons and nuclei. In general, electrons and ions are coupled together. In solid state physics such a coupling is weak in most cases, because electrons and ions move under different time scales. The heavier ions are then treated classically while the lighter electrons quantum mechanically. Electrons are said to evolve adiabatically around ions. This separation is justified on the basis of the Born-Oppenheimer(BO) adiabatic approximation.

Let's first write the total Hamiltonian as

$$h = T_N + T_e + V \tag{2.3}$$

where T_N and T_e are the kinetic energy operators for ions and electrons respectively, and V includes the various contributions to the potential energy. We then expand the total wave function as the product

$$\varphi = \sum_i \chi_i \psi_i \tag{2.4}$$

where the $\{\chi_i\}$'s are expansion coefficients (depending on $\{R_I\}$), and the electronic state ψ_i is the i-th eigenstate of $H = T_e + V$

$$H\psi_i = E_i\psi_i \tag{2.5}$$

Of course, here ψ_i itself is a many-body wave function. Since the ionic coordinates $\{\vec{R}_I\}$ enter H as parameters, E_i's and ψ_i's depend on $\{\vec{R}_I\}$ parametrically. By substituting the expansion (2.4) into the Schrödinger equation $h\varphi = \epsilon\varphi$, multiplying it by ψ_i^* and integrating over the electronic degrees of freedom, we obtain an equation which the function $\chi_i(\{\vec{R}_I\})$ satisfies

$$(T_N+E_i)\chi_i = \epsilon\chi_i - \sum_{j(\neq i)} \sum_I \frac{1}{M_I} < \psi_i|\vec{P}_I|\psi_j > \cdot\vec{P}_I\chi_j - \sum_j < \psi_i|T_N|\psi_j > \chi_j \tag{2.6}$$

Here we have used the explicit expression $T_N = \sum_I \frac{\vec{P}_I^2}{2M_I}$ where $\vec{P}_I$ and M_I are the momentum and mass of the I-th ion. Since usually the typical ionic frequencies are much smaller than the electronic ones and the ionic masses are much larger than ionic ones, the non-adiabatic interactions, i.e. the second and the third terms on the right hand of Eq.(2.6), can be neglected[17]. Eq.(2.6) then becomes

$$(T_N + E_i)\chi_i = \epsilon\chi_i \tag{2.6a}$$

In addition, it is most frequently possible to use classical mechanics to describe the ionic motion since ionic energy spectra are usually almost continuous compared with the electronic ones. Thus the eigen-energy E_i of the electrons acts as ionic potential Φ in Eq.(2.1). This is a surface spanned in a $3N$-dimensional space. In particular we shall refer to the ground-state energy as to the BO surface.

According to Eq.(2.5), the electrons follow the ionic motion in an adiabatic way. However Eq.(2.5) is a many-body problem. It is not a trivial task to solve it. Within DF-LDA[15], the many-electron problem is conveniently converted to many one-electron problems, in which the electron moves in a self-consistent effective single-particle field.

2.3 Electronic Ground State at a Fixed Ionic Configuration

According to DF theory, the total ground-state energy $\Phi[\{\vec{R}_I\}]$ of a system of interacting electrons and ions, corresponding to the ionic configuration $\{\vec{R}_I\}$, is a unique functional of the electronic density $n(\vec{r})$. This can be written in terms of occupied one-electron orthonormal orbitals

as

$$n(\vec{r}) = \sum_{i}^{occ} |\psi_i(\vec{r})|^2 \tag{2.7}$$

For a fixed set of $\{\vec{R}_I\}$, the ground-state energy can be obtained by minimizing the functional $E[\{\psi_i\}, \{\vec{R}_I\}]$ with respect to the 'electronic degrees of freedom' $\{\psi_i\}$

$$\Phi[\{\vec{R}_I\}] = \min_{\{\psi_i\}} E[\{\psi_i\}, \{\vec{R}_I\}] \tag{2.8}$$

where the functional $E[\{\psi_i\}, \{\vec{R}_I\}]$ is given by

$$E[\{\psi_i\}, \{\vec{R}_I\}] = \sum_{i}^{occ} \int d\vec{r} \psi_i^*(\vec{r})(-\frac{1}{2}\nabla^2)\psi_i(\vec{r}) + \int d\vec{r} V^{ext}(\vec{r}) n(\vec{r}) +$$

$$+\frac{1}{2}\int\int d\vec{r} d\vec{r}' \frac{n(\vec{r})n(\vec{r}')}{|\vec{r}-\vec{r}'|} + E^{xc}[n] + \frac{1}{2}\sum_{I\neq J} \frac{Z_I Z_J}{|\vec{R}_I - \vec{R}_J|} \tag{2.9}$$

and the $\{\psi_i\}$'s are subject to the orthonormality constraints

$$\int d\vec{r} \psi_i^*(\vec{r})\psi_j(\vec{r}) = \delta_{ij} \tag{2.10}$$

In Eq.(2.9), atomic units (a.u.) $e = \hbar = m_e = 1$ are used for convenience. V^{ext} is the external field, $E^{xc}[n]$ is the exchange-correlation energy and Z_I's are the charges of the ionic cores. To reach the ground state, one proceeds by minimizing the total energy with respect to a trial wave function of electrons. This amounts to solving

$$\frac{\delta E}{\delta \psi_i^*} = 0 \tag{2.11}$$

with the constraints (2.10). This yields the so-called Kohn-Sham (KS) equations

$$H\psi_i \equiv [-\frac{1}{2}\nabla^2 + V^{ext}(\vec{r}) + \int d\vec{r}' \frac{n(\vec{r}')}{|\vec{r}-\vec{r}'|} + \frac{\delta E^{xc}}{\delta n}]\psi_i(\vec{r}) = \varepsilon_i \psi_i(\vec{r}) \tag{2.12}$$

Eqs. (2.12) must be solved self-consistently since the Hartree $V_H \equiv \int d\vec{r}' \frac{n(\vec{r}')}{|\vec{r}-\vec{r}'|}$ and exchange-correlation $\mu^{xc} \equiv \frac{\delta E^{xc}}{\delta n}$ potentials depend themselves on the $\{\psi_i\}'$s. The self-consistent solution is usually obtained by iterative diagonalisations, after expanding the $\{\psi_i\}'$s on a suitable basis set.

More recently however, a different way of solving Eq.(2.8) has been pointed out[18]. This is to simply find the local minimum of $E[\{\psi_i\}, \{\vec{R}_I\}]$ by a steepest descent(SD) approach

$$\begin{aligned} \dot{\psi}_i(\vec{r},t) &= -\frac{\delta E}{\delta \psi_i^*(\vec{r},t)} + \textit{orthonormality constraints} \\ &\equiv -H\psi_i(\vec{r},t) + \textit{orthonormality constraints} \end{aligned} \tag{2.13}$$

The orthonormality constraints can be satisfied using either the Gram-Schmidt scheme or the Lagrangian multiplier scheme. Remark that neglecting the constraints, Eq.(2.13) can be formally thought as a time-dependent Schrödinger equation in imaginary time. Starting from an initial trial state $\tilde{\psi}_i$, the ground state ψ_i can be obtained using

$$\psi_i(\vec{r}) = \lim_{t\to\infty} e^{-\int_0^t H dt} \tilde{\psi}_i(\vec{r},t) + \textit{orthonormality constraints} \tag{2.14}$$

For large systems, this SD scheme is more convenient than the traditional diagonalization techniques because only the occupied states are taken into account. Recently, minimization procedures similar to SD but significantly faster from the computational point of view have been developed[19,20].

2.4 *ab-initio* Molecular Dynamics

As pointed out in the first section of this chapter, one of the most important problems in classical MD is the determination of the interac-

tion potential between the atoms. This problem is particularly serious for open shell systems, where the interaction depends strongly on the electronic configuration. An accurate and at the same time practical solution to this problem has been proposed a few years ago by Car and Parrinello[5]. In the so-called Car-Parrinello(CP) method, the electronic and ionic degrees of freedom are treated simultaneously. For each ionic configuration $\{R_I\}$, the interatomic potential is obtained directly from the electronic ground state calculated within DF theory. The electrons move adiabatically along the ionic trajectory, i.e. they are always in the ground state (or very close to it) corresponding to the instantaneous $\{R_I\}$. The adiabatic motion of the coupled electron-ion system is achieved by introducing a fictitious classical system described by the Lagrangian

$$L = \sum_i \frac{1}{2}\mu \int d\vec{r}|\dot{\psi}_i|^2 + \sum_I \frac{1}{2}M_I|\dot{\vec{R}}_I|^2 - E[\{\psi_i\},\{\vec{R}_I\}]+ \\ + \sum_{ij}\Lambda_{ij}\int d\vec{r}(\psi_i^*\psi_j - \delta_{ij}) \qquad (2.15)$$

where the $\{\psi_i\}$'s and $\{R_I\}'$ refer to the electronic and ionic degrees of freedom respectively, Λ is an Hermitian matrix of Lagrangian multipliers introduced to impose the orthonormality constraints Eq.(2.10), $E[\{\psi_i\},\{\vec{R}_I\}]$ is the functional given by Eq.(2.9) which acts as the potential energy of the generalized system, and μ is a fictitious mass associated with the electronic degrees of freedom. The choice of μ is such that it is sufficiently smaller than the ionic masses to ensure the adiabatic motion of the electrons.

The Lagrangian (2.15) generates a dynamics for $\{\psi_i\}$'s and $\{\vec{R}_I\}$'s

through the equations of motion,

$$\mu\ddot{\psi}_i(\vec{r},t) = -\frac{\delta E}{\delta\psi_i^*(\vec{r},t)} + \sum_j \Lambda_{ij}\psi_j(\vec{r},t) \qquad (2.16a)$$

$$\equiv -H\psi_i + \sum_j \Lambda_{ij}\psi_j(\vec{r},t)$$

$$M_I\ddot{\vec{R}}_I = -\nabla_{\vec{R}_I}E \qquad (2.16b)$$

where H is the KS hamiltonian (2.12).

In this coupled system, the energy $U = K_e + K_I + E$, where $K_e = \sum_i \frac{1}{2}\mu\int d\vec{r}|\dot{\psi}_i|^2$ and $K_I = \sum_I \frac{1}{2}M_I|\dot{\vec{R}}_I|^2$ are classical kinetic energies for electronic and ionic degrees of freedom respectively, is conserved since the orthonormality constraints are just time-independent holonomic constraints and hence do not do work[22]. K_e is much smaller than K_i if electrons are very close to the ground-state. In this case, $U_I = K_I + E$ is approximately constant and very close to U. In all systems (both insulators and metals), however, the Lagrangian (2.15) will eventually lead to final equilibration between electrons and ions, *i.e.* energy transfer from the ionic to the electronic subsystem. During such a process, K_e increases continuously and, correspondingly, the ionic trajectories deviate from the BO surface. In insulators, by appropriate choice of μ and initial conditions ($\{\psi_i(t=0)\}$, $\{\dot{\psi}_i(t=0)\}$), it is possible to make the equilibration time so long that practically no energy transfer occurs during typical MD simulation times. In metals, vice versa, some energy transfer occurs on a relatively small time scale in spite of the choice of μ and of the initial conditions. In order to maintain the adiabaticity of the ionic motion, one has therefore to perform periodic minimizations to bring the electrons on the ground-state. Correspondingly, because of the energy loss in K_I, one should couple the

ions to some external reservoir in order to maintain the temperature at the required value. In this work the ionic temperature is kept constant by using the scheme which was proposed a few years ago by Nosè[30] and which is described in detail in appendix A.

For the numerical calculations, the Verlet algorithm[21] has been shown to be very efficient. Eqs.(2.16) are thus rewritten as

$$\psi_i(t+\Delta t) = -\psi_i(t-\Delta t) + 2\psi_i(t) + f_i\frac{\Delta t^2}{\mu} \qquad (2.17a)$$

$$\vec{R}_I(t+\Delta t) = -\vec{R}_I(t-\Delta t) + 2\vec{R}_I(t) + \vec{F}_I\frac{\Delta t^2}{M_I} \qquad (2.17b)$$

where f_i and $\vec{F}_I$ are the forces appearing on the right hands of Eqs.(2.16a) and (2.16b) respectively. The forces on the ions are calculated by using the Hellmann-Feynman theorem

$$-\nabla_{\vec{R}_I} E = - < \Psi^0 | \nabla_{\vec{R}_I} H | \Psi^0 > \qquad (2.18)$$

where Ψ^0 is the ground state of the many-electron system. Thus the interionic forces are derived directly from the electronic ground state and the ions move along the BO surface.

Chapter 3

Technical Aspects: Pseudopotentials for Ga and As and the Kleinman-Bylander Scheme

3.1 General Discussion

The usual procedure of solving the Schrödinger equation

$$H\psi_i \equiv (T+V)\psi_i = \varepsilon_i \phi_i \tag{3.1}$$

is by expanding the unknown wave function ψ_i on a given basis $\{\phi_j\}$ (usually being orthonormal)

$$\psi_i = \sum_j c_j^i \phi_j \tag{3.2}$$

The eigenvalues ε_i and the $\{c_j^i\}$ are then obtained either by solving the secular equation

$$\| H_{kj} - \varepsilon_i \delta_{kj} \| = 0 \tag{3.3}$$

where $H_{kj} = < \phi_k | H | \phi_j >$, or using the SD method described in the last chapter. In many cases, it is convenient to choose a plane wave(PW) basis set

$$\phi_{\vec{G}}^{\vec{k}}(\vec{r}) = \frac{1}{\sqrt{\Omega}} e^{i(\vec{G}+\vec{k}).\vec{r}} \tag{3.4}$$

where Ω is the volume of the system, $\vec{k}$ is a representative point in the first Brillouin zone(BZ) and $\vec{G}$ is a reciprocal lattice vector. Eq.(3.2) then becomes

$$\psi_{\vec{k}} = \sum_{\vec{G}} c_{\vec{G}}^{\vec{k}} \phi_{\vec{G}}^{\vec{k}} \tag{3.5}$$

and Eq.(3.3) can be expressed in Fourier space:

$$\| [\frac{1}{2}(\vec{G} - \vec{k})^2 - \varepsilon_{\vec{k}}] \delta_{\vec{G},\vec{G}'} + V_{\vec{G},\vec{G}'} \| = 0 \tag{3.6}$$

In practice, the plane wave expansion (3.5) has to be truncated at a suitable size (i.e. $\frac{1}{2} G_{max}^2 \leq Ecut$). Since electron-ion Coulomb interactions are very strong at small $\vec{r}(\sim r^{-1})$, an exceedingly large number of PW's are in principle required to represent electrons strongly localized around the core of the nuclei. Pseudopotential theory [23] has been introduced to eliminate this disadvantage. Pseudopotentials describe the interaction of an electron outside the ionic core region (a region with $r < r_c$, where r_c is the "core radius") with the ion(nucleus plus cloud of core electrons) and should yield the same physical properties as the true potential. Instead of the strong attractive potential at small r, pseudopotentials are smooth inside the core region but for valence states they yield the same eigenvalues as the ones given by the real potential.

Because of the smoothness of pseudopotentials, a relatively small number of PW's is sufficient to describe a real system. Until some time ago pseudopotentials were usually obtained either by adjusting Fourier expansion coefficients to agree with some experimentally determined features of the energy bands or by fitting model potentials to atomic energy values. More recently a first-principle approach has been introduced for the construction of pseudopotentials. The so-called Norm Conserving Pseudopotentials(NCPS)[24] belong to the category of the first-principle pseudopotentials. They have the following desirable properties:

(1) Real and pseudo valence eigenvalues agree for a chosen "prototype" atomic configuration.

(2) Real and pseudo atomic wave function agree beyond r_c.

(3) The integrals from 0 to r of the real and pseudo charge densities agree for $r > r_c$ for each valence state (norm conserving).

(4) The logarithmic derivatives of the real and pseudo wave function and their first energy derivatives agree for $r > r_c$.

The last two properties ensure that NCPS have optimum transferability among a variety of chemical environments.

In general, pseudopotentials can be broken into local and nonlocal(NL) parts, *i.e.*

$$\hat{V}_{ps} = V_{loc}(\vec{r}) + V_{NL}(\vec{r}, \vec{r}') \tag{3.7}$$

$$\hat{V}_{NL}\phi(\vec{r}) = \int V_{NL}(\vec{r}, \vec{r}')\phi(\vec{r}')d\vec{r}' \tag{3.8}$$

and usually only the orientation is involved in this non-locality. Therefore $\hat{V}_{NL}$ can be expressed as

$$\hat{V}_{NL} = \sum_l v_l(r)\hat{P}_l. \tag{3.9}$$

Here $\hat{P}_l$ is the projection operator which projects out the l-th angular momentum component $\phi_l(\vec{r})$ from the function $\phi(\vec{r})$

$$\phi_l(\vec{r}) \equiv \sum_m \chi_{lm}(r) Y_{lm}(\theta, \varphi) = \hat{P}_l \phi$$

where $Y_{lm}(\theta, \varphi)$ is a spherical harmonic function. The explicit form of $\hat{P}_l$ is

$$\hat{P}_l = \sum_m Y_{lm}(\theta, \varphi) Y^*_{lm}(\theta', \varphi') \tag{3.10}$$

$$\hat{P}_l \phi(\vec{r}) = \sum_m Y_{lm}(\theta, \varphi) \int Y^*_{lm}(\theta', \varphi') \phi(\vec{r}') \sin\theta' d\theta' d\varphi'. \tag{3.11}$$

It can be shown that

$$\sum_l \hat{P}_l = 1 \tag{3.12}$$

In practice, high l components of the wave function are negligible. In Eq.(3.9), we can assume

$$v_l(r) = v_{ref}(r) \qquad for \quad l > l_{max} \tag{3.13}$$

where l_{max} is some truncated l value and v_{ref} is a reference function. Using eqs.(3.12) and (3.13), Eq.(3.9) becomes

$$\hat{V}_{NL} = v_{ref}(r) + \sum_{l=0}^{l_{max}} \Delta v_l \hat{P}_l \tag{3.14}$$

where $\Delta v_l = v_l - v_{ref}$. The first term on the right hand is a local operator and hence can be put into V_{loc} of Eq.(3.7), leaving the rest as the pure NL part.

Using a PW basis set, the matrix element of the pseudopotentials (3.7) becomes

$$V_{\vec{G},\vec{G}'} = V_{loc}(\vec{G} - \vec{G}') + V_{NL}(\vec{G}, \vec{G}') \tag{3.15}$$

where the explicit expression of $V_{NL}(\vec{G}, \vec{G}')$ is [25]

$$V_{NL}(\vec{G}, \vec{G}') = \sum_l \frac{4\pi}{\Omega}(2l+1) P_l(\cos(\theta_{\vec{G},\vec{G}'})) \int_0^\infty dr r^2 j_l(Gr) j_l(G'r) \Delta v_l(r) \tag{3.16}$$

where P_l is a Legendre polynomial, $\theta_{\vec{G},\vec{G}'}$ is the angle between the vectors $\vec{G}$ and $\vec{G}'$ and j_l is a spherical Bessel function.

For each pair of $\vec{G}$ vectors, the two terms on the right hand side of (3.15) are obtained by two different integrals. It appears that an n-dimensional (n PW's) matrix needs $2n$ integrals for the local terms and $\frac{n}{2}(n+1)$ integrals for the NL ones. As the number of PW employed grows, the calculation of the NL term becomes very demanding. This is the case especially for systems containing a large number of atoms.

Kleinman and Bylander(KB)[26] proposed a factorized form for the NL pseudopotentials

$$\hat{V}_{NL} = \sum_{l}^{l_{max}} \sum_{m} \frac{|\Delta v_l \Phi^0_{lm} >< \Phi^0_{lm} \Delta v_l|}{< \Phi^0_{lm}|\Delta v_l|\Phi^0_{lm} >} \tag{3.17}$$

where Φ^0_{lm} is the atomic pseudo wave function corresponding to the pseudopotential of Eq.(3.7). It is noticeable that $\hat{V}_{NL}|\Phi^0_{lm} >= \Delta v_l|\Phi^0_{lm} >$, *i.e.* factorized and unfactorized NL pseudopotentials are equivalent under the state Φ^0_{lm}. By the replacement (3.17), the number of integrals for $V_{NL}(\vec{G},\vec{G}')$ is n rather than $\frac{n}{2}(n+1)$. Explicitly

$$V_{NL}(\vec{G},\vec{G}') = \sum_{l} \frac{4\pi}{\Omega}(2l+1)P_l(\cos(\theta_{\vec{G},\vec{G}'}))\int_0^\infty dr r^2 j_l(Gr)\phi_l(r)\Delta v_l(r)\times$$

$$\times \int_0^\infty dr r^2 j_l(G'r)\phi_l(r)\Delta v_l(r) / \int_0^\infty dr r^2 [\phi_l(r)]^2 \Delta v_l(r) \tag{3.18}$$

Here $\phi_l(r)$ is the radial part of Φ^0_{lm}.

The KB scheme reduces significantly the effort of calculating the NL pseudopotential elements. It is found however that the accuracy of the scheme depends strongly on the choice of the reference function in Eq.(3.13). In the following we shall present the results of several tests aimed at finding an appropriate reference potential for the KB scheme in GaAs.

3.2 Testing the KB scheme for c-GaAs

In the present work, the NCPS obtained by Bachelet *et al*[27] are employed for Ga and As where 1s2s2p3s3p3d are dealt with as core states. We perform our tests on crystalline GaAs (c-GaAs) since self-consistently diagonalising the Hamiltonian of such a small system (only two atoms per unit cell) is very economical. For a given choice of the reference potential of Ga and As, we calculated the energy eigenvalues by both using the unfactorized formula (3.16) (we denote these results as "exact") and the KB scheme. The $\vec{k}$ points in the first BZ used to represent the charge density within the DF scheme are those which fold into the Γ-point of the cubic supercell of 64 atoms used in our calculations with the CP method (see section 4.1). Very similar eigenvalues are obtained with a converged set of special k-points[28]. An energy cutoff of 14 Ry ($\sim$140 PW's per atom) was used for wavefunctions, while a cutoff of 14$\times$1.58 Ry=22.12 Ry was found sufficient to represent the charge density and the potential. This choice yields reasonably well converged energy eigenvalues[28] (with a lower energy cutoff, *e.g.* 12 Ry, the calculated energy gap of c-GaAs is found to become indirect). Our results are given in Table 3.1.

We tested two different reference potentials, i.e. $v_{ref} = v_2$ (d-potential) and $v_{ref} = v_1$ (p-potential). In the first case $v_{NL} = \Delta v_0 \hat{P}_0 + \Delta v_1 \hat{P}_1$ (we denote it as sp-NL) whereas in the second case $v_{NL} = \Delta v_0 \hat{P}_0 + \Delta v_2 \hat{P}_2$ (we denote it as sd-NL). From Table 3.1, we can see that, unlike the "exact" results, the KB scheme is quite sensitive to the choice of the reference potential. In the sp-NL case, the KB results deviate appreciably from the "exact" ones. The most important dif-

ference occurs for the energy gap between the valence and conduction bands ($\Gamma_1 - \Gamma_{15}$), which is only ~ 0.25 the value of the "exact" one. Of course, the "exact" itself is smaller than the experiment due to the

Table 3.1:

Energies (in eV) at some selected k-points for c-GaAs, obtained by the "exact" and the KB scheme. The sixth column reports experimental results[28].

	sp-NL		sd-NL		
$\vec{k}$	exact	KB	exact	KB	Exp.
Γ_1	-12.56	-12.69	-12.55	-12.55	-13.1
Γ_{15}	0	0	0	0	0
Γ_1	0.62	0.15	0.63	0.72	1.42
Γ_{15}	3.75	3.77	3.75	3.76	
X_1	-10.14	-10.13	-10.13	-10.13	-10.75
X_3	-6.72	-6.79	-6.72	-6.72	-6.70
X_5	-2.59	-2.57	-2.59	-2.58	-2.80
X_1	1.41	1.03	1.41	1.43	1.81
X_3	1.61	1.46	1.61	1.62	2.38
X_5	10.15	10.16	10.16	10.17	
L_1	-10.90	-10.94	-10.89	-10.89	-11.24
L_1	-6.54	-6.57	-6.54	-6.53	-6.70
L_3	-1.09	-1.08	-1.09	-1.09	-1.30
L_1	1.03	0.54	1.04	1.08	1.72
L_3	4.62	4.62	4.62	4.62	5.41
L_1	7.68	5.26	7.70	7.71	

local-density approximation(LDA). From Table 3.1 it is evident that the KB scheme with sd-NL is a better choice. However, this choice is com-

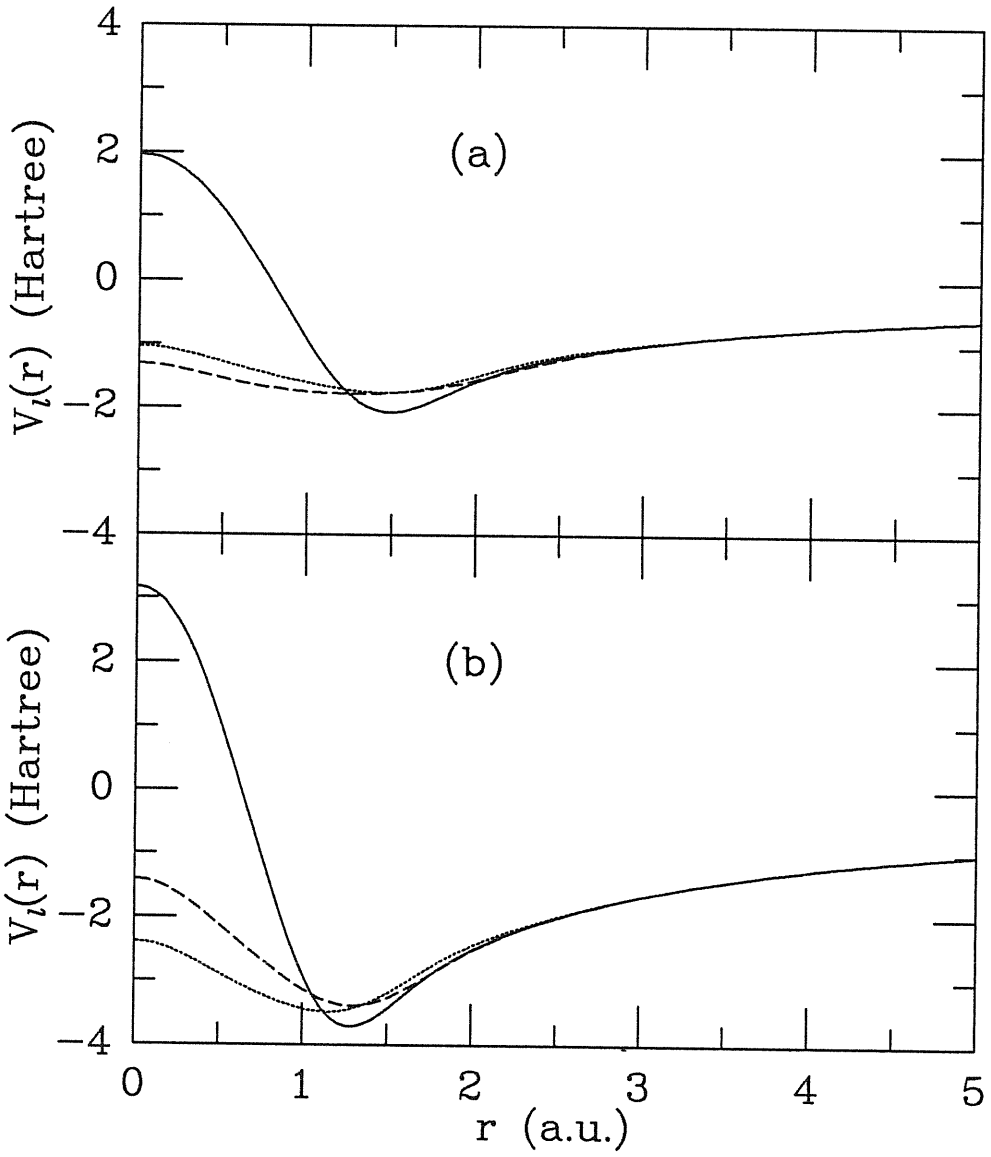

Figure 3.1:

NL terms of the Pseudopotential for: (a) Ga and (b) As[27]. The full, dashed and dot line correspond $l = 0$, 1 and 2 respectively.

putationally costly because the calculation of the NL pseudopotential matrix elements is proportional to $(2l+1)$.

In Fig.3.1 we show the NL terms of the pseudopotential, v_l, for Ga

Table 3.2: Energies (in eV) of c-GaAs at some selected k-points using sp-NL for As and only s-NL for Ga. The three columns refer to three different treatments of the NL pseudopotential. The symbol in parentheses denotes which wave function is used in KB formula

$\vec{k}$	exact	KB(Φ^0_{lm})	KB($\tilde{\Phi}_{lm}$)
Γ_1	-12.32	-12.30	-12.28
Γ_{15}	0	0	0
Γ_1	0.86	1.09	1.01
Γ_{15}	3.94	3.95	3.95
X_1	-9.96	-9.96	-9.95
X_3	-6.52	-6.53	-6.53
X_5	-2.38	-2.38	-2.39
X_1	1.44	1.49	1.47
X_3	1.64	1.65	1.65
X_5	10.30	10.20	10.21
L_1	-10.70	-10.70	-10.68
L_1	-6.32	-6.32	-6.33
L_3	-0.97	-0.96	-0.97
L_1	1.19	1.28	1.25
L_3	4.64	4.64	4.64
L_1	7.85	7.83	7.84

and As. It appears that the $v_2(r)$ and $v_1(r)$ potentials for Ga are quite close. We approximately take $v_2 \simeq v_1$ for Ga, and thus treat Ga as s-NL but As as sp-NL. The results of the test for this choice are listed in Table 3.2. It appears that the KB results are quite close to the "exact" ones. This choice, which has the advantage of being rather accurate and computationally convenient, is the one which we shall adopt in the following.

3.3 Using the KB scheme for *ab-initio* molecular dynamics

The systems we are interested in are usually much larger than the elementary cell of a crystal. The number of PW, n, is therefore large compared with that used for the crystal calculation. In these case it is undoubtedly convenient to use the factorized KB scheme to calculate the NL pseudopotentials matrix elements. One possible drawback of using the KB scheme within the CP method is related to the denominator of Eq.(3.17). As described in the last chapter, $H\psi$ works as the force on the electronic degrees of freedom. If one or more denominators in the KB formula happen to be very small, V_{NL}(Eq.3.18), and hence H, will become very large in magnitude. In the numerical solution of the equations of motion, such as Eq.(2.18a), Δt must then be restricted to very small values in order to get an accurate solution. This makes the calculations more costly and somehow offsets the advantage of the KB scheme. This case happens indeed for As when we use v_2 or v_1 as the reference potential.

The justification of the KB scheme is based on the fact that when the

KB-NL pseudopotential acts on the atomic state Φ^0_{lm}, it is equivalent to the "exact" one

$$\frac{|\Delta v_l \Phi^0_{lm} >< \Phi^0_{lm} \Delta v_l|}{< \Phi^0_{lm} |\Delta v_l| \Phi^0_{lm} >} |\Phi^0_{lm} >= |\Delta v_l \Phi^0_{lm} > \tag{3.19}$$

In practice, however, the atomic state Φ^0_{lm} is represented in PW's

$$\Phi^0_{lm}(\vec{r}) = \sum_{\vec{G}} c^0_{\vec{G}} e^{i\vec{G}.\vec{r}} \tag{3.20}$$

and truncated at some G_{max}

$$\tilde{\Phi}^0_{lm}(\vec{r}) = \sum_{\vec{G}=0}^{G_{max}} c^0_{\vec{G}} e^{i\vec{G}.\vec{r}} \tag{3.21}$$

It appears that in order to satisfy the equality (3.19) *all* Φ^0_{lm} appearing in the KB factorized potential must be changed consistently to $\tilde{\Phi}^0_{lm}$. We found that when this is done, also the "denominator problem" mentioned above is largely removed. In the 3rd column of Table 3.2, we report selected eigenvalues of c-GaAs calculated using the KB-$\tilde{\Phi}$ scheme. It appears that the comparison with both the KB using true atomic states and the "exact" scheme is very favorable.

The effect of the different forms of NL pseudopotentials can be illustrated by the calculated lattice constants of c-GaAs. The lattice constant, computed employing s-NL for Ga and sp-NL for As is ~10.35 a.u., *i.e.* 3% smaller than the experimental value (10.68 a.u.[29]), whereas if both Ga and As are treated as sp-NL the lattice constant is ~10.45 a.u., *i.e.* 2% smaller than the experiment(the same results are found both with the "exact" and the KB schemes). We see no essential difference.

Chapter 4

Liquid GaAs

The first-principle molecular dynamics (CP) method is used to simulate a liquid GaAs(l-GaAs) system. A detailed picture of the atomic and electronic structure of the liquid is obtained.

4.1 Technical Details

A cubic MD cell containing 64 (32 Ga and 32 As) atoms with periodic boundary conditions is used. The cell size is chosen as 20.864 a.u., giving the experimental density at the melting point, $\rho \sim 5.71 gr\ cm^{-3}$[1]. The electronic wave functions at the Γ-point in the first BZ are expanded in plane waves with a kinetic energy cut-off of 14 Ry. Norm conserving pseudopotentials[27] within the local-density approximation(LDA)[15] are used together with Kleinman and Bylander's factorized form of the non-local pseudopotentials(see ch.3). Due to the reason explained in Chapter 3, s-nonlocality for Ga and sp-nonlocality for As are adopted.

To prepare a liquid system, the atoms are initially arranged in a zinc-blende crystal structure with some random displacement, and are then

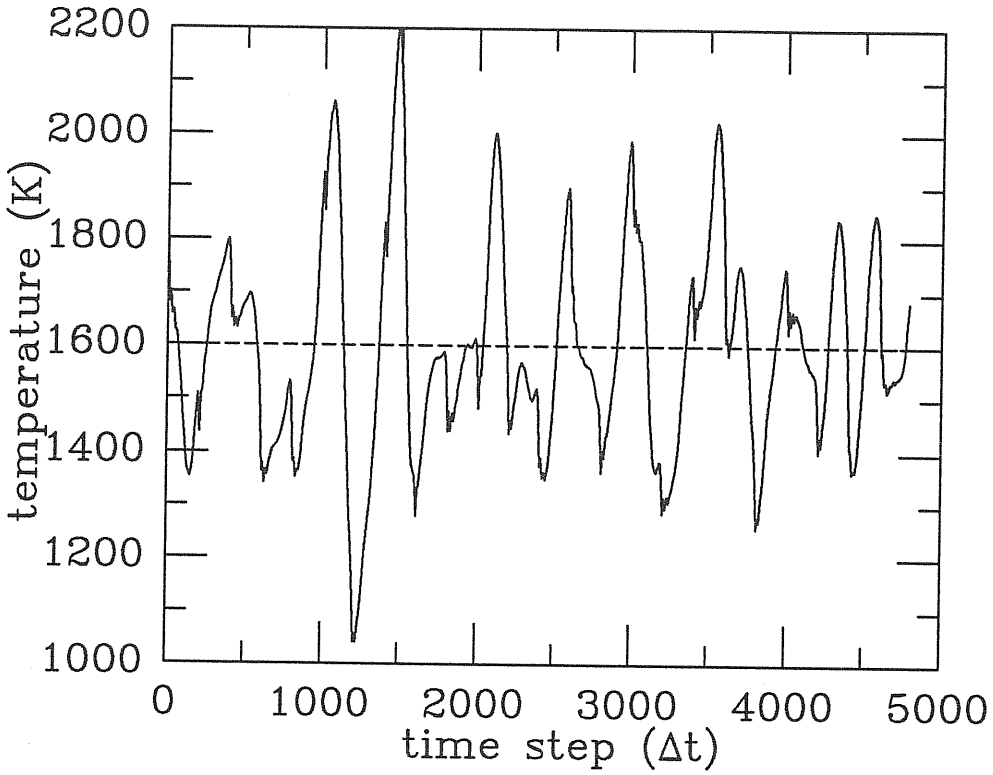

Figure 4.1: The instantaneous temperature(full line) during the simulation fluctuates around the equilibrium temperature(dashed line).

relaxed. The temperature of the system is gradually raised (by rescaling the ionic velocities) up to 3000K to ensure a molten system. This is indicated by the diffusing behavior of the mean square displacement. The temperature is then gradually reduced to ~1600K, a little bit above the experimental melting point 1511K. The system is equilibrated at this temperature for a few thousand time steps.

When applying the CP method to a metallic system such as *l*-GaAs, an energy transfer from the ionic to the electronic degrees of freedom can take place within a rather short time scale, as already discussed in chapter 2. This implies a deviation from the ground-state BO surface,

or a thickness of the BO surface. We found that using a time step Δt=15 a.u. ($\sim 3.6\times10^{-16}$sec.) and the fictitious mass parameter of the electronic degrees of freedom μ=7500 a.u., it was sufficient to perform a systematic minimization of the electrons every 200 Δt. Within this time scale, the thickness of the BO surface is $\sim$100K, much smaller than the equilibrium temperature of the real system.

The statistical atomic configurations are collected for 4800 time steps ($\sim$1.72 ps.). The temperature is kept constant (in average) by coupling the ions to two thermostats (one is for Ga and another is for As), as proposed by Nosè[30] for a purely classical system, giving a canonical ensemble statistics (NVT). A detailed description of this procedure is given in appendix A. The instantaneous temperature shown in Fig.4.1 always oscillates around the equilibrium temperature during the simulation.

4.2 Structural Properties

The most basic characteristic of a disordered system, such as a liquid or a glass, is that it possesses short-range order, differing from the long-range periodicity of a crystal. The X-ray or neutron diffraction pattern are still important experimental ways to determine the structure. The static structure factor $S(k)$, which is the Fourier transform of the pair correlation function $g(r)$

$$S(k) = 1 + \rho \int_0^\infty 4\pi r^2 [g(r) - 1] \frac{\sin kr}{kr} dr \qquad (4.1)$$

where ρ=N/V is the average number density of N atoms in volume V, is related to the intensity of the scattering $I(k)$ by

$$S(k) = \frac{I(k)}{Nf(k)^2}. \tag{4.2}$$

Here $f(k)$ is the scattering form factor of an individual atom and k is the momentum transfer. The pair correlation function $g(r)$ is defined by setting $4\pi\rho r^2 g(r)dr$ equal to the total number of atoms in a spherical shell of radius r and thickness dr centered on a given atom, which can give us a direct microscopic picture of the short-range order. The relation between the two-particle distribution

$$\rho^{(2)}(\vec{r}_1, \vec{r}_2) \equiv \sum_{I \neq J}^{N} \delta(\vec{r}_1 - \vec{R}_I)\delta(\vec{r}_2 - \vec{R}_J) \tag{4.3}$$

and $g(r)$ ($r = |\vec{r}_1 - \vec{r}_2|$) is

$$< \rho^{(2)}(\vec{r}_1, \vec{r}_2) >= \rho^2 g(r) \tag{4.4}$$

where the bracket $< \cdots >$ denote the statistical average. Considering the translational invariance of the system, we obtain

$$\begin{aligned} \rho g(r) &= \frac{1}{N} < \sum_{I \neq J} \delta\{\vec{r} - (\vec{R}_I - \vec{R}_J)\} > \\ &= \frac{1}{N} < \sum_I \sum_J \delta\{\vec{r} - (\vec{R}_I - \vec{R}_J)\} > -\delta(\vec{r}) \end{aligned} \tag{4.5}$$

By Fourier transformation, we can also get

$$S(k) = \frac{1}{N} < \sum_{I,J} e^{i\vec{k}\cdot(\vec{R}_I - \vec{R}_J)} > \tag{4.6}$$

In a two-component system, Ashcroft and Langreth[31](AL) proposed the following definition for the partial pair correlation functions and partial structure factors,

$$c_\beta \rho g_{\alpha\beta}(r) = \frac{1}{N_\alpha} < \sum_I^{N_\alpha} \sum_J^{N_\beta} \delta\{\vec{r} - (\vec{R}_{\alpha I} - \vec{R}_{\beta J})\} > -\delta_{\alpha\beta}\delta(\vec{r}) \tag{4.7}$$

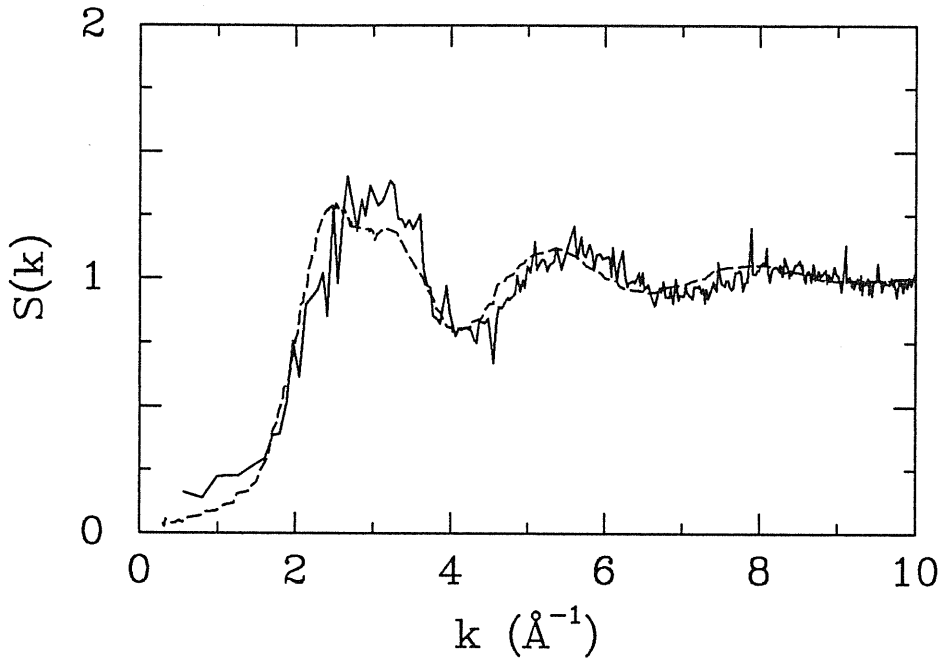

Figure 4.2:

The structure factor of liquid GaAs. The full line is the present result and the dashed line is the result from the neutron scattering experiment.[2]

$$S_{\alpha\beta}(k) = (N_\alpha N_\beta)^{-1/2} < \sum_I^{N_\alpha} \sum_J^{N_\beta} exp\{-i\vec{k}\cdot(\vec{R}_{\alpha I} - \vec{R}_{\beta J})\} > -(N_\alpha N_\beta)^{-1/2}\delta_{\vec{k},0} \tag{4.8}$$

where N_α is the number of α-type atoms and $c_\alpha = N_\alpha/N$ is the respective number concentration.

From the ionic coordinates of the configurations collected in the simulation, by using Eqs.(4.7) and (4.8), we obtain the partial pair correlation functions $g_{\alpha\beta}(r)$ (Fig.4.3b) and the partial structure factors (α =Ga, As; β =Ga, As). To compare our results with the neutron scattering experiment[2], we should combine the partial $S_{\alpha\beta}(k)$ with the

experimental neutron scattering lengths b_α as follows

$$S(k) = \frac{b_{Ga}^2 S_{GaGa}(k) + 2b_{Ga}b_{As}S_{GaAs}(k) + b_{As}^2 S_{AsAs}(k)}{(b_{Ga} + b_{As})^2} \tag{4.9}$$

where b_{Ga}=7.2 and b_{As}=6.7[32]. The comparison for the structure factor $S(k)$ is shown in Fig.4.2. The agreement between theory and experiment is very good. The calculated $S(k)$ is a little bit noisy because of the limited configurations collected. Like l-Si and l-Ge, the first peak is accompanied by a shoulder at higher k value. The small shift of the calculated $S(k)$ to higher k-value with respect to the experiment is due to the theoretical underestimate of the Ga-As equilibrium bond length which was mentioned in chapter 3.

Better insight into the structure of the liquid is provided by $g(r)$. In Fig.4.3a, the experimental $g(r)$, which was obtained by Fourier transformation of the experimental $S(k)$, and our result are shown. We notice that the theoretical $g(r)$ is obtained by combining the partial $g_{\alpha\beta}(r)$—which are calculated directly in r space—with the b'_αs, in a way similar to that of Eq.(4.9). A noticeable feature of both curves in Fig.4.3a is the almost complete absence of structure beyond the first neighbor peak. This feature is usually attributed to non-compact structures, since in these systems the structure is not "nested" shell by shell. It also appears that, in spite of an inward shift which is corresponds to the outward shift in $S(k)$, the theoretical peak reproduces quit well the height and width of the experiment. From the area below the first peak of $g(r)$, one can estimate the average coordination number Z in the liquid. By fitting the first peak with two Gaussians, we find Z=5.0, whereas by direct integration of $4\pi\rho r^2 g(r)$ up to the first minimum at $r_{min} \sim 3.26$ $\mathring{A}$, we find Z=6.3. The corresponding experimental value is Z=5.5$\pm$0.5, the

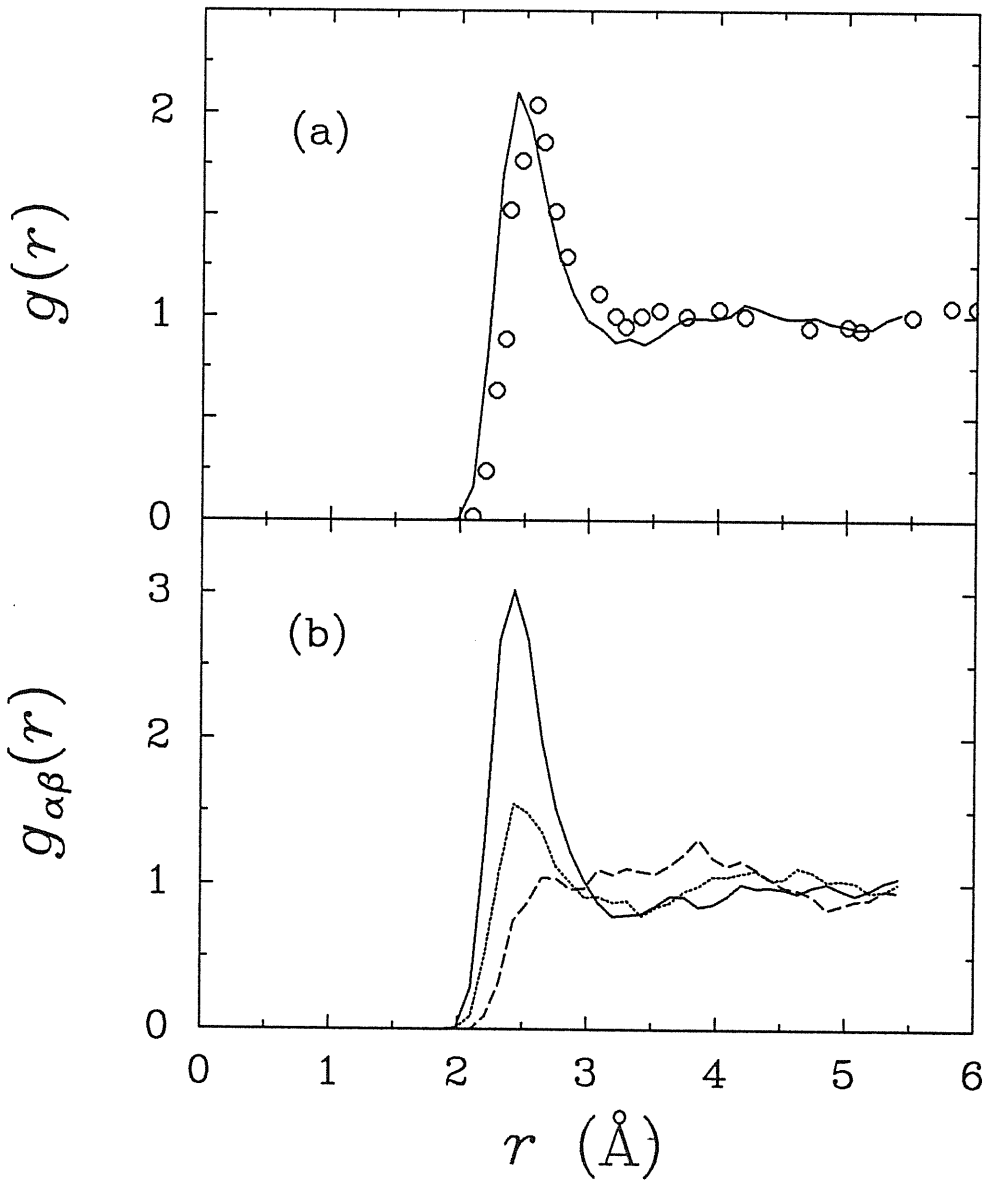

Figure 4.3: (a) The pair correlation function $g(r)$, where the circles denote the experimental one; (b) the partial correlation functions. Full line: Ga-As. Dashed line: AsAs. Dotted line: Ga-Ga.

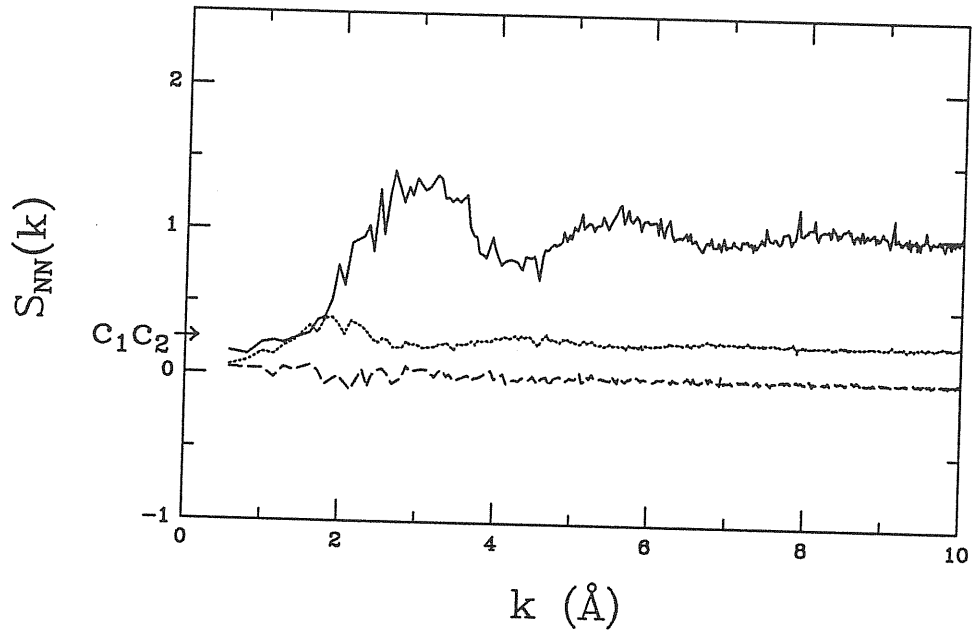

Figure 4.4: The number-concentration structure factors. The full line is S_{NN}, the dot line is S_{CC} and the dashed line is the cross term S_{NC}.

incertitude being related to the procedure used to analyse the first peak.

The calculated partial pair correlation function $g_{\alpha\beta}(r)$ are shown in Fig.4.3b. Unfortunately, experimental results for these quantities are not available, although in principle they can be obtained by scattering through isotopic substitution. In a strongly ionic system, such as molten salts, peaks and minima of $g_{\alpha\beta}(r)$ for like-atoms are out of phase with respect to those of unlike-atoms, reflecting the characteristic alternation of cation and anion shells. This is not the case in Fig. 4.3b, indicating a strong covalent character for the binding in l-GaAs. The probability of finding a like-atom in the nearest neighbor shell of one atom is appreciable. By integrating to r_{min}, each Ga/As has on the average 2.6/2.2 and 3.9 neighbors of the like- and unlike-species respectively.

In Fig.4.4 we show the Bhatia and Thornton's[33] partial structure

factors which are obtained from their relationships with the AL's partial structure factors. These are the mean-square fluctuations in the particle number, the concentration and their cross term, *i.e.*

$$S_{NN}(k) = \frac{1}{N} < N^*(\vec{k})N(\vec{k}) > \qquad (4.10a)$$

$$S_{CC}(k) = N < C^*(\vec{k})C(\vec{k}) > \qquad (4.10b)$$

$$S_{NC}(k) = Re < N^*(\vec{k})C(\vec{k}) > . \qquad (4.10c)$$

Here $N(\vec{k})$ and $C(\vec{k})$ are Fourier components of the local fluctuations of the number density

$$\Delta\rho(\vec{r}) = \rho(\vec{r}) - \bar{\rho} \qquad (4.11)$$

and the concentration

$$\Delta c(\vec{r}) = c(\vec{r}) - \bar{c} \qquad (4.12)$$

respectively. Their relationships to the AL's partial structure factors $S_{\alpha\beta}(k)$ are[34]

$$S_{NN}(k) = c_1 S_{11}(k) + c_2 S_{22}(k) + 2(c_1 c_2)^{1/2} S_{12}(k) \qquad (4.13a)$$

$$S_{CC}(k) = c_1 c_2 [c_2 S_{11}(k) + c_1 S_{22}(k) - 2(c_1 c_2)^{1/2} S_{12}(k)] \qquad (4.13b)$$

$$S_{NC}(k) = c_1 c_2 [S_{11}(k) - S_{22}(k) + (c_2 - c_1) S_{12}(k)/(c_1 c_2)^{1/2}] \qquad (4.13c)$$

where c_1 and c_2 are the concentrations of the two different species 1 and 2 ($c_1 + c_2 = 1$). From Fig.4.4, it appears that $S_{NN}(k)$ is almost equivalent to $S(k)$ of Fig.4.2, and $S_{CC}(k)$ has a peak at about 1.8 $\AA^{-1}$, about half of the position of the first peak of $S_{NN}(k)$, revealing a tendency to an alternative arrangement of atoms although it is not as pronounced as that in a pure ionic system.

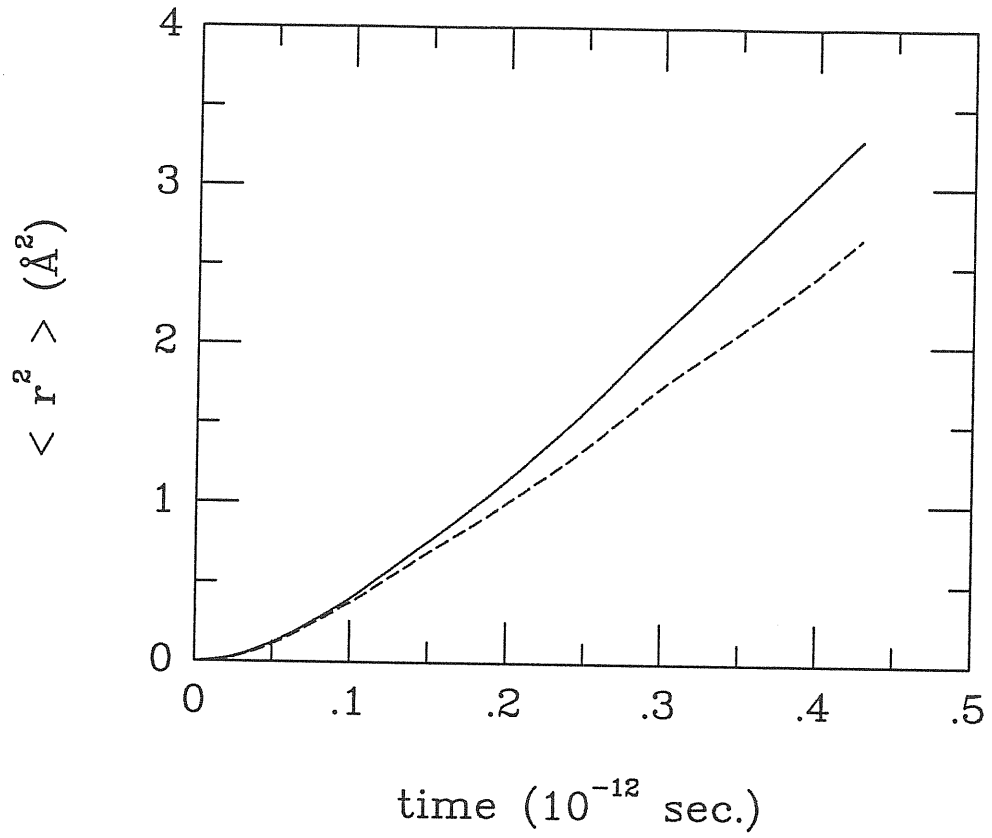

Figure 4.5: The mean square displacements of Ga(full line) and As(dashed line). They are averaged over 10 different starting points.

4.3 Dynamical Properties

Also the dynamical properties of the liquid are well described by our simulation. The diffusion coefficients of Ga and As can be evaluated from the large t behavior of mean square displacements by Einstein relation

$$D = \lim_{t \to \infty} < r^2 > /6t \tag{4.14}$$

as $D_{Ga} = 1.6 \times 10^{-4}$ and $D_{As} = 1.2 \times 10^{-4}\ cm^2 s^{-1}$ respectively. The experimental value, which does not distinguish between the two different species, is $D_{GaAs} = 1.6 \times 10^{-4}\ cm^2 s^{-1}$ at $T \sim 1550K$[35]. The auto-

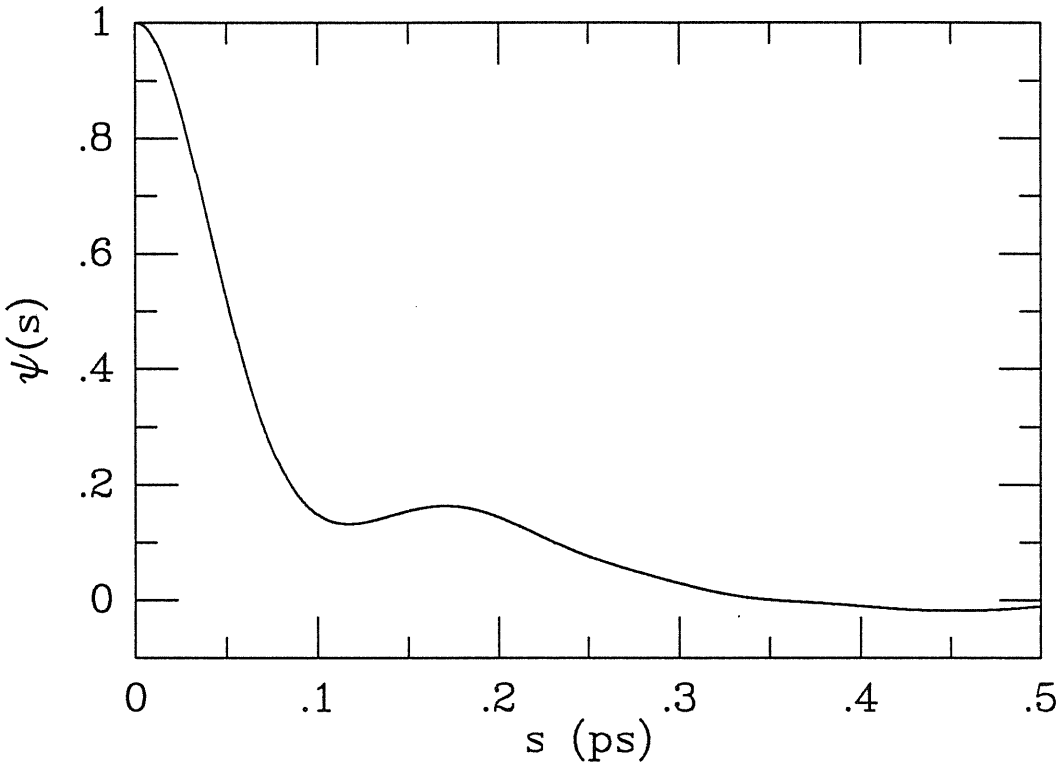

Figure 4.6: The auto-correlation function of atomic velocities for l-GaAs.

correlation function of the atomic velocity

$$Z(s) = \frac{< \vec{V}(t) \cdot \vec{V}(t+s) >}{< \vec{V}(t) \cdot \vec{V}(t) >} \tag{4.15}$$

is shown in Fig.4.6. The diffusion coefficient estimated from this function coincides with that from Einstein relation. The vibrational density of states spectrum $D(\omega)$ is obtained by Fourier transformation of $Z(s)$, *i.e.*

$$D(\omega) \propto \int_0^\infty Z(t) \cos(\omega t) dt, \tag{4.16}$$

and is shown in Fig.4.7. A shoulder occurs at about $\omega \sim 25THz$ which should be related to the optical phonon peak in the crystal. This value is $\omega \sim 50THz$ at zero temperature. As temperature rises, it will shift to lower value. Unfortunately no experimental data near the melting point seem availabe.

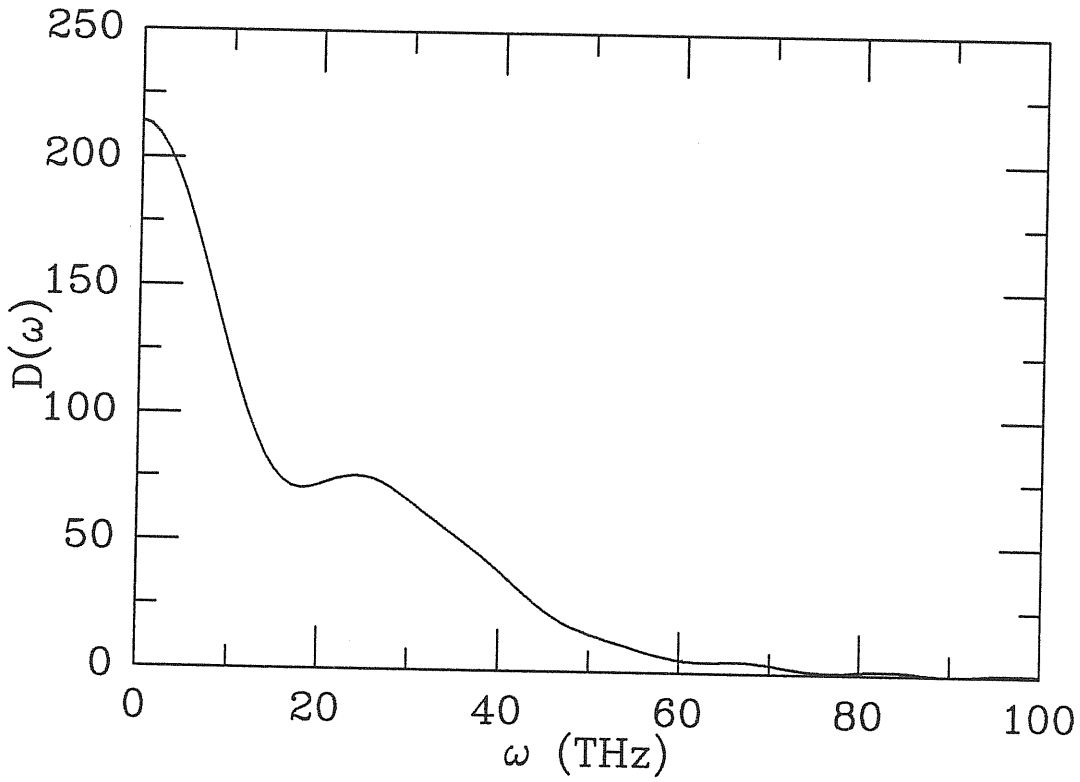

Figure 4.7: The vibrational density of states for l-GaAs. The unit for $D(\omega)$ is arbitrary.

4.4 Bonding

It is interesting to obtain a microscopic picture of bonding in l-GaAs. By studying the electronic charge distribution between an atom and its surrounding neighbors, we find that not all the atoms at distances $r \leq r_{min}$ are bonded to the central atom. This point is illustrated in Fig.4.8 where we show contour plots of the charge density for a few typical configurations in the liquid, as compared to the charge density (in a (110) plane) of c-GaAs (4.8a). Actually the covalent bonds are not present if the interatomic distance d exceeds some d_{cov}, which we approximately estimate as $d_{cov} \sim 2.65\mathring{A}$, *i.e.* $\sim 10\%$ larger than the equilibrium bond length for c-GaAS (we assume the same d_{cov} for all types of bond, although the average As-As separation is found to be slightly larger than the Ga-As and Ga-Ga ones). By integrating $g(r)$ up to d_{cov} we obtain that the average number of bonds formed by each atom is ~ 2.9, implying that about 50% of the atoms within the distance r_{min} are not bonded to the central atom.

A similar indication is provided by the behavior of the bond-angle-distribution(AD), as illustrated in Fig.4.9. The figure shows the total AD calculated using two different values of the cut-off distance R_c, namely $R_c = r_{min}$ and $R_c = d_{cov}$(dashed line). A significant difference between the two curves is remarkable. It appears that the curve with $R_c = d_{cov}$ has a pronounced peak at $\theta \sim 109°$, *i.e.* the bond-angle of c-GaAs, whereas for the curve with $R_c = r_{min}$ the peak has become broader and shifted to $\theta \sim 100°$, while at the same time a second feature at $\theta \sim 54°$ has emerged. The latter corresponds to configurations where at least one atom within r_{min} is not bonded to the central one.(see lower

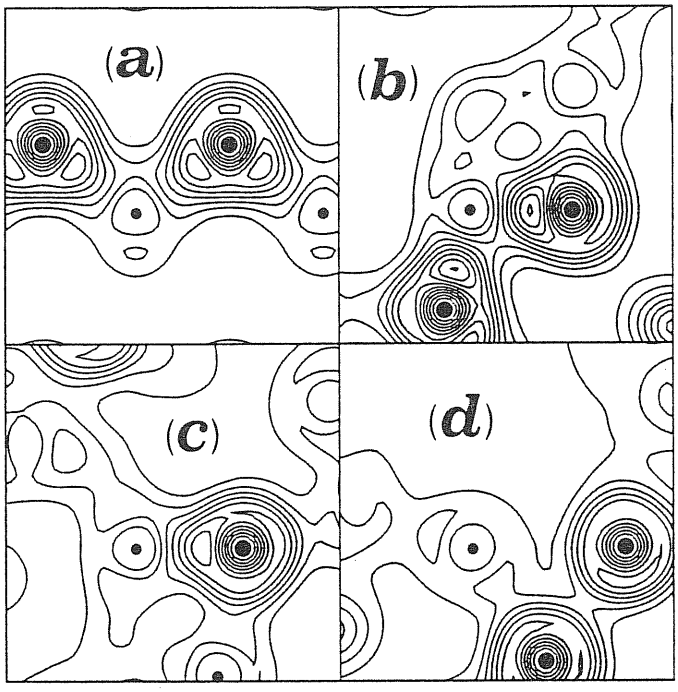

Figure 4.8:

Contour plots of the valence electronic charge density for some configurations. Small and large dots denote Ga and As ions respectively. (a) charge density in the (110) plane of c-GaAs (bond length d_c=2.45 Å). (b), (c), (d) are some selected configurations of the liquid. In (b), both As atoms form bonds with the Ga atom at the center (bond distances: $d_1 \simeq d_2 = 2.14\mathring{A}$). In (c) the As atom bonds to the Ga on the left ($d_1 = 2.21\mathring{A}$) while it does not form a bond with the Ga at the bottom ($d_2 = 2.70\mathring{A}$). In (d) the Ga atom does not form bonds with either As ($d_1 = 3.22\mathring{A}$, $d_2 = 2.81\mathring{A}$).

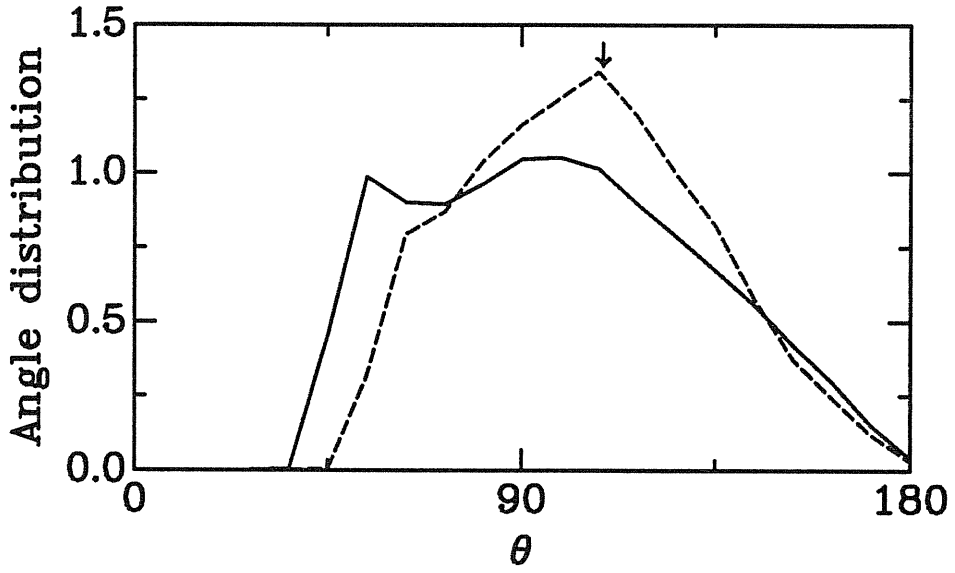

Figure 4.9: Total bond angle distribution calculated using two different values of the cut-off distance R_c, $R_c = r_{min}$(full line) and $R_c = d_{cov}$(dashed line). The vertical arrow denotes the value of the tetrahedral angle, 109°.

panels of Fig. 4.8)

Charge density contour plots for several bonding configuration in the liquid are shown in Fig. 4.10, including "crystal-like" configurations such as (a) and (d), wrong bonds such as in (b) and (e), and three atom "clusters" as in (c) and (f). The "crystal like" configurations of type (a) and (d) are the prominent configurations, but configurations like (b) and (e) also occur frequently. We find statistically that about 18% and 9% of the total number of bonds are Ga-Ga and As-As respectively. The probability of the "three-atom cluster" configurations (c) and (f) is instead significantly lower (4% and 2% respectively). Fig.4.11 shows the relative probability for different number of atoms in a "cluster". It

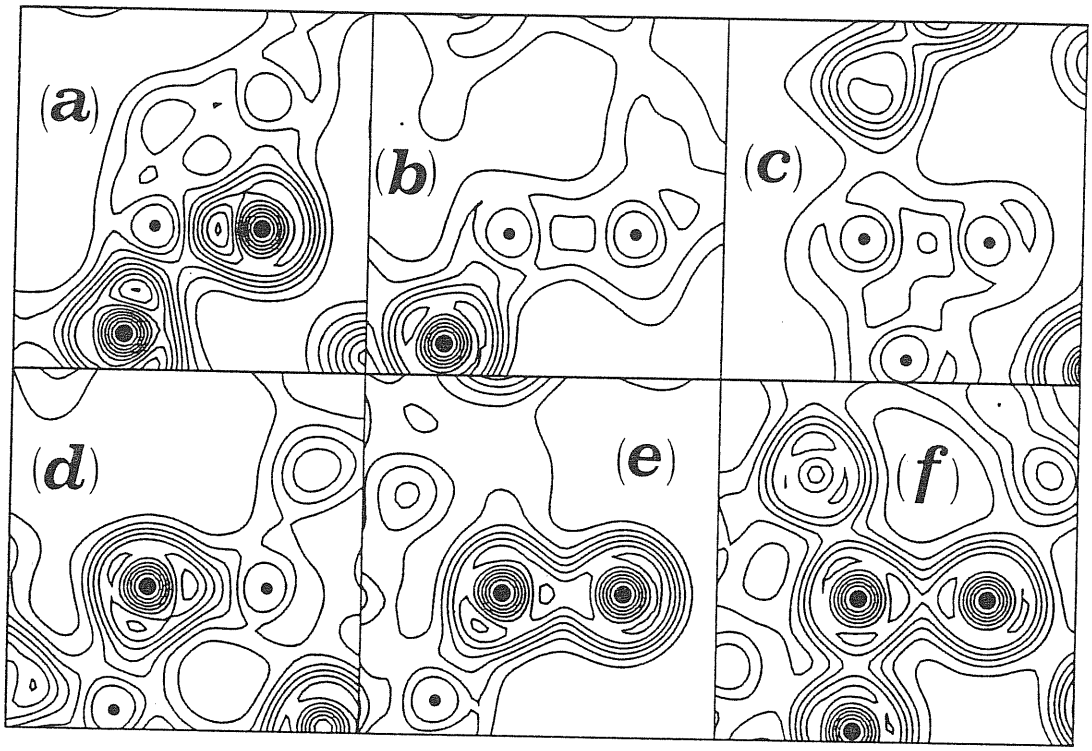

Figure 4.10: Contour plots of the valence electronic charge density in l-GaAs for different atomic configurations: (a) Ga-As-Ga; (b) Ga-Ga-As; (c) Ga-Ga-Ga; (d) Ga-As-Ga; (e) As-As-Ga; (f) As-As-As. The small and large dots denote Ga and As ions respectively.

decays quickly as the number of atoms increase. "Clusters" with atoms larger than 4 only occur occasionally.

The charge density plots in Fig.4.10 also show that the Ga-As bond in the liquid is weakly ionic, as in the crystal. The Ga-Ga bonds show a small pile-up of charge at the center, similar to that observed in orthorombic c-Ga[36]. Finally, the As-As bond is dominated by p elec-

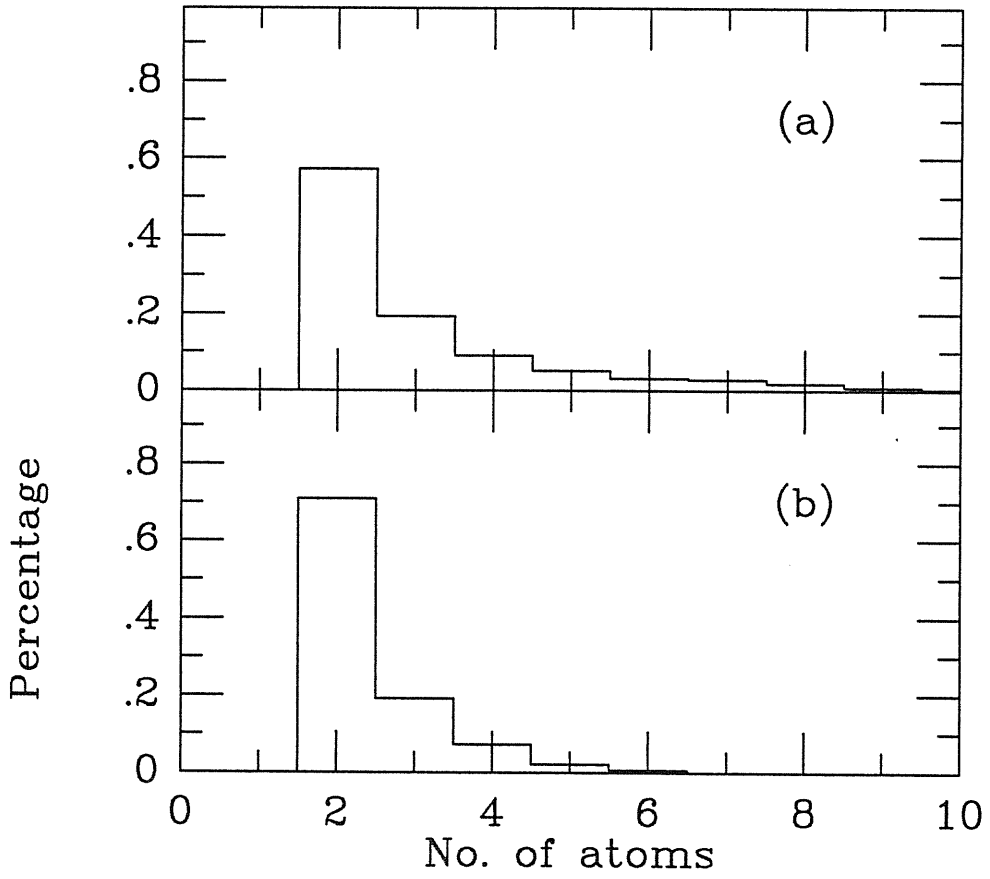

Figure 4.11: The relative probability for like-atom "clusters" of different size: (a) Ga; (b) As.

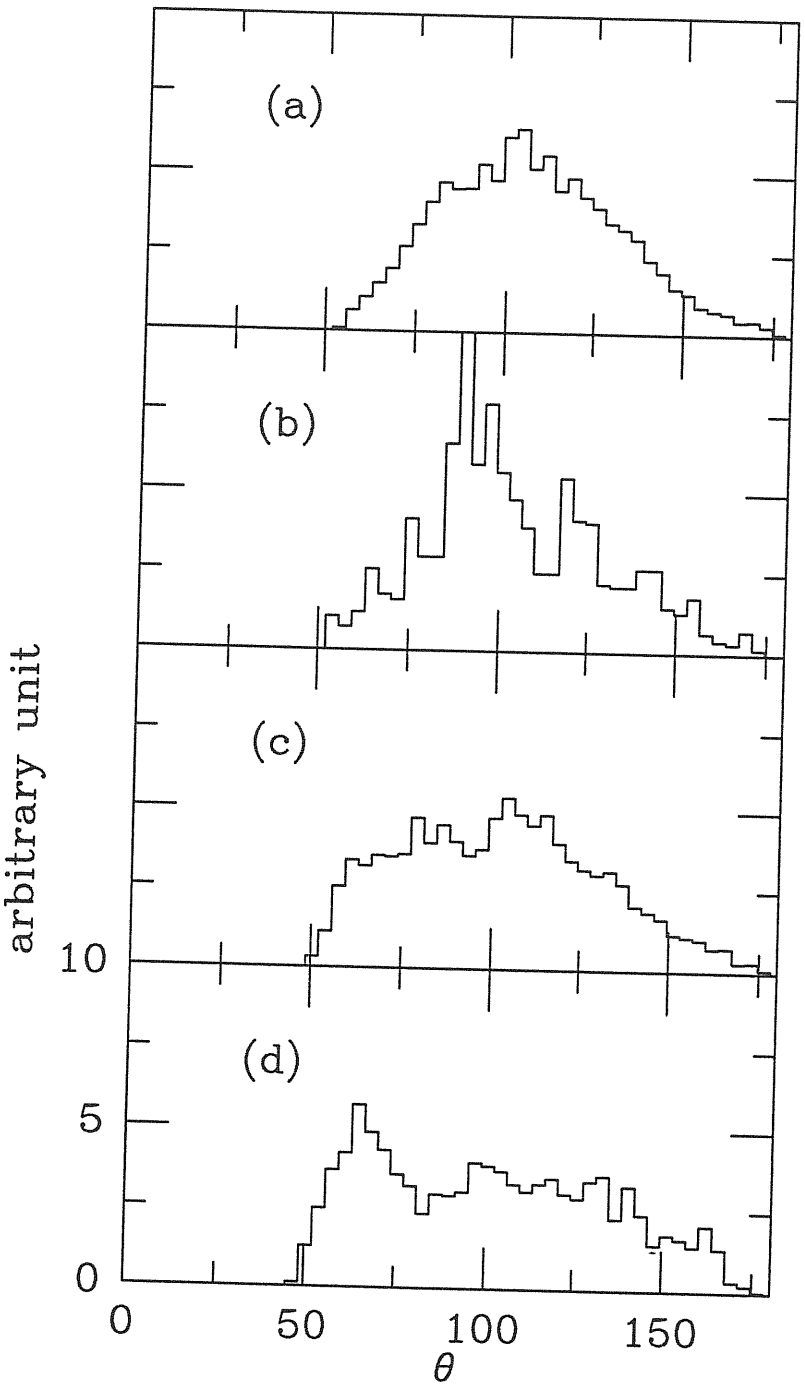

Figure 4.12: Partial bond angle distribution (calculated with $R_c = d_{cov}$) for: (a)AsGaAs; (b) AsAsAs; (c) GaAsGa; (d) GaGaGa.

trons as found in c-As[37]. Fig. 4.12 shows the partial AD corresponding to configurations like those in Figs.4.10(a), (c), (d) and (f). The distributions are wide spread. The AD for AsGaAs has a peak centered at $\sim 105°$, i.e. rather close to the tetrahedral angle of 109°; the AD for AsAsAs which is relatively noisy due to less statistics, has a sharp peak at $\sim 95°$, in agreement with that in pure l-As[38]. Finally Figs.4.12(c) and (d) show that when two Ga atoms bond with a central atom (Ga/As), the AD's are quite flat, suggesting weak interactions between the two Ga atoms.

4.5 Electronic Properties

To obtain the electronic properties, such as the single-particle density of states $D(E)$ and the electrical conductivity $\sigma(\omega)$, the empty single-particle states above the Fermi level are taken into account. These are calculated for 12 different ionic configurations, using an SD procedure similar to that of Eq.(2.13)(where however the electronic density $n(r)$ is fixed).

$D(E)$ for l-GaAs is shown in Fig.4.13 where results for c-GaAs are also displayed for comparison. Some similarity in the main features of the two curves is visible. Also in the liquid, for instance, there is at low energies, between ~ -12 and $\sim -8eV$, the band of s-like states originating from the As atoms. In the liquid, however, $D(E)$ is finite at the Fermi level E_f, thus indicating that this is metallic, in agreement with the experimental transport data[1]. The localization of single-particle states increases smoothly along the band, as shown by the behavior of

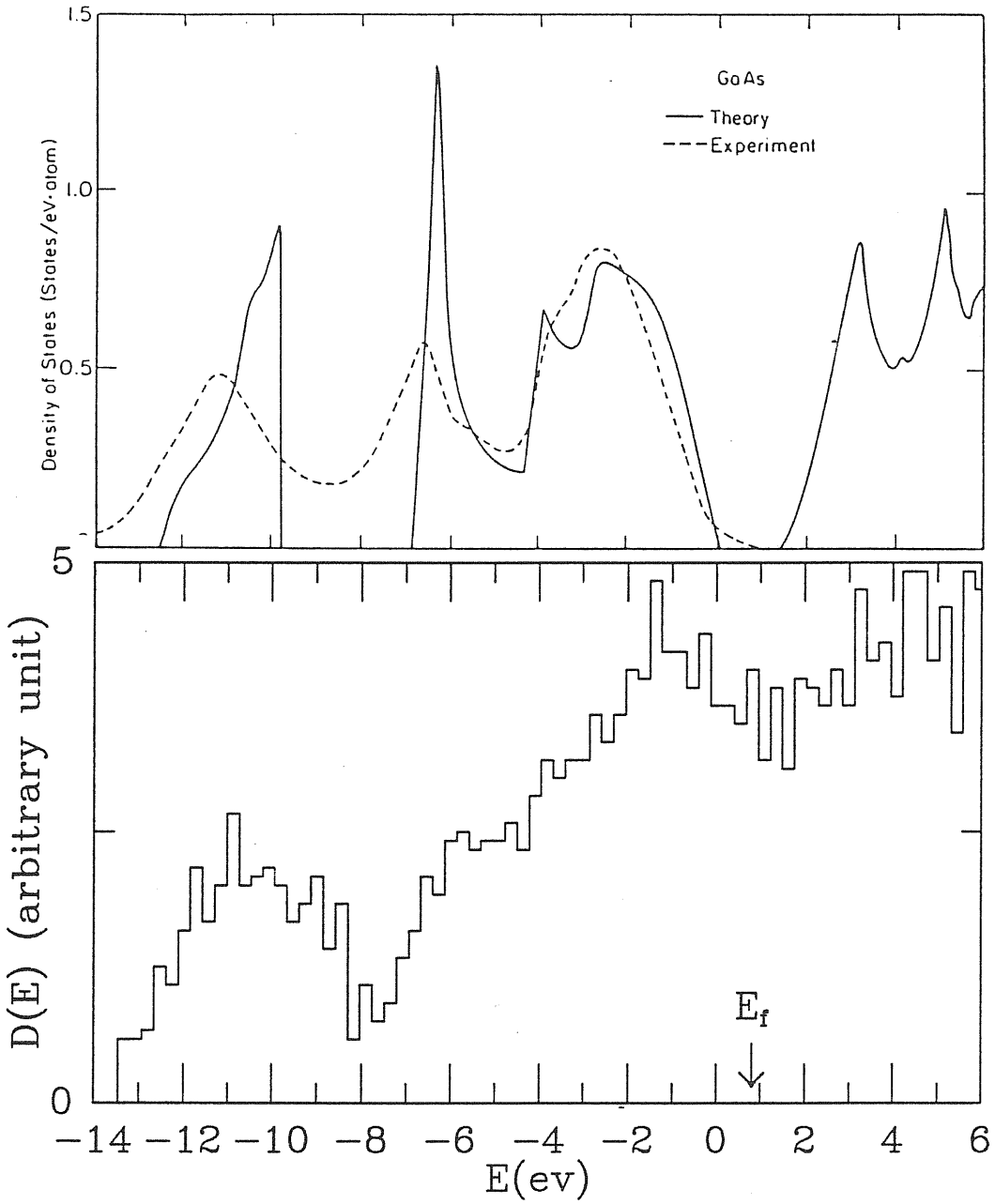

Figure 4.13:

The single particle electronic density of state $D(E)$. The upper panel is the result for c-GaAs, from [39]. The lower panel is for l-GaAs, where the vertical arrow denotes the position of the Fermi energy.

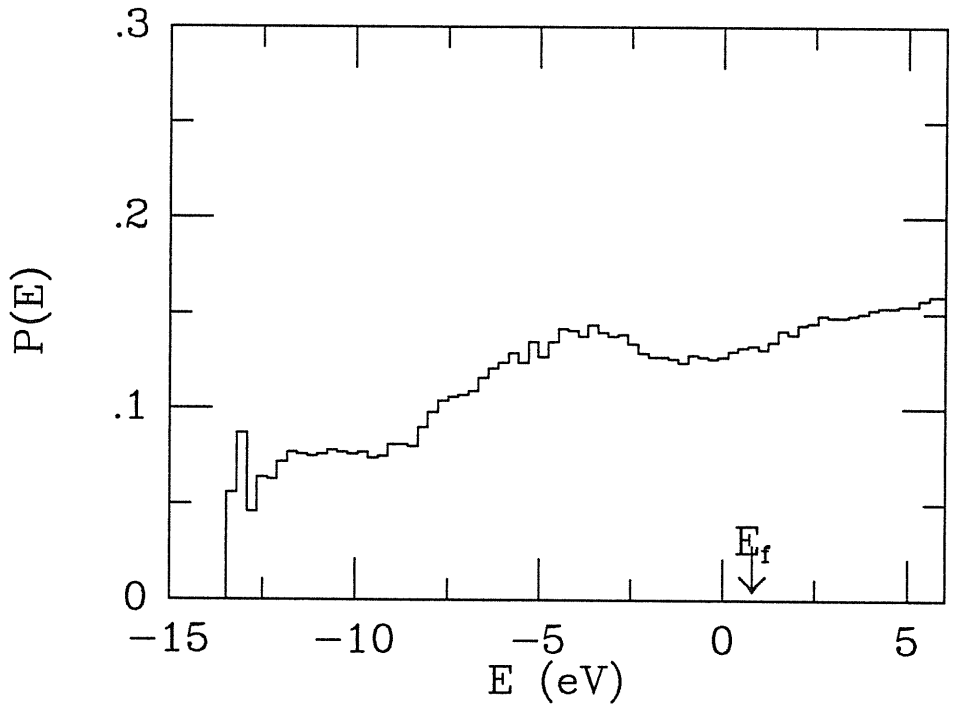

Figure 4.14: The participation ratio

the participation ratio $P(E)$, shown in Fig.4.14. $P(E)$ is defined as

$$P(E) = \frac{1}{\Omega} \sum_i \frac{[\int |\psi_i|^2 d\vec{r}]^2}{\int |\psi_i|^4 d\vec{r}} \delta(E - E_i) \tag{4.17}$$

where Ω is the volume of the MD cell, ψ_i a single-particle state and E_i is its eigen-energy. For a pure plane wave state, $P(E) = 1$ at that point, whereas for a localised δ-function state $P(E) = 0$.

In Fig.4.15, we show the electrical conductivity $\sigma(\omega)$ calculated as the configurational average of [40]

$$\sigma(\omega, \{\vec{R}_I\}) = \frac{2\pi e^2}{m^2 \omega} \frac{1}{\Omega} \sum_{m,n} | < \psi_m \mid \hat{P} \mid \psi_n > |^2 \delta(E_n - E_m - \hbar\omega) \tag{4.18}$$

where $\{\vec{R}_I\}$ denotes the given ionic configuration and $\hat{P}$ is the momen-

tum operator. The lowest 256 Kohn-Sham states are used for each set of $\{\vec{R}_I\}$, *i.e.* twice the number of occupied states. We remark that the use of these states to describe single-particle properties is not well justified[41] and thus introduces an additional approximation, beside the Franck-Condon approach implicit in the use of BO states in Eq.(4.18). The calculated value $\sim 7500\Omega^{-1}cm^{-1}$ of the static d.c. conductivity, obtained by extrapolating $\sigma(\omega)$ to zero frequency, is in remarkable agree-

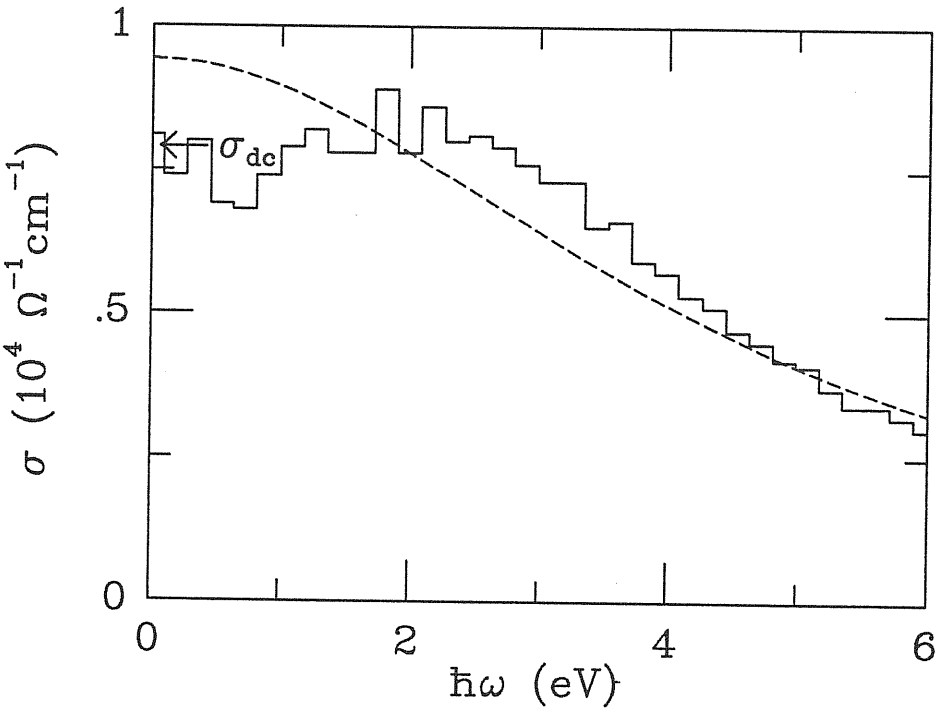

Figure 4.15: The electrical conductivity $\sigma(\omega)$ of l-GaAs (full line). The horizontal arrow indicates the experimental value of the d.c. conductivity. The dashed line is obtained by approximately fitting the calculated curve with Drude formula.

ment with the experimental value of $\sim 7900\Omega^{-1}cm^{-1}$[1]. In the classical Drude model, the real part of conductivity is

$$\sigma(\omega) = \frac{\sigma(0)}{1+\omega^2\tau^2}.$$

A crude fitting of this formula to our results is shown as the dashed line in Fig 4.15. From the fitting, we obtain the values $\sigma(0)$ $\sim$9400 $\omega^{-1}cm^{-1}$ and $\tau \sim 9.4 \times 10^{-16}$ sec. Although there is no available experimental value of τ to compare with, the τ obtained from the fitting is of the same order of magnitude as that of l-Si ($\tau \sim 2.2 \times 10^{-16}$ sec[43]). From Fig.4.15, it appears that the Drude model does not describe well the conductivity of l-GaAs at energies below $\sim$2eV, thus suggesting significant deviations from free electron-like behavior. This is in contrast with the situation in l-Si[44], where Drude formula gives a very good description of the conductivity at all energies. This different behavior is also observed in the single particle density of states: this looks significantly more free electron-like in l-Si[44] than in l-GaAs.

In summary, a first-principle MD simulation has been performed on the liquid GaAs. The physical quantities obtained are in good agreement with experiments. Although the coordination number increases after melting, not all the atoms in the first coordination shell bond with the central atom. Each atom has $\sim$ 2.9 bonds on average, less than that in the crystal. These broken bonds contribute to the increase of the electrical conductivity.

Chapter 5

Simulated Quenching of GaAs

A crystal phase corresponds to the global minimum of the multidimensional potential energy surface, while an amorphous phase is metastable, *i.e.* associates with local but relative stable minima of the surface. Experimentally amorphous semiconductors are usually produced by evaporation , rf glow discharge or sputtering. Freezing from the liquid phase in fact does not give rise to amorphous systems, since the cooling rates which can be achieved experimentally are not sufficiently fast to prevent crystallisation. In a MD simulation, however, it is possible to quench a liquid so rapidly that an amorphous solid rather than a crystal is obtained. In this chapter, the CP method is used in a numerical simulated quenching to obtain an amorphous GaAs sample from the corresponding liquid.

We start from the equilibrium liquid described in chapter 4. The temperature is reduced from 1600 K to room temperature(300 K). At present however this process has not been completed yet. The results of

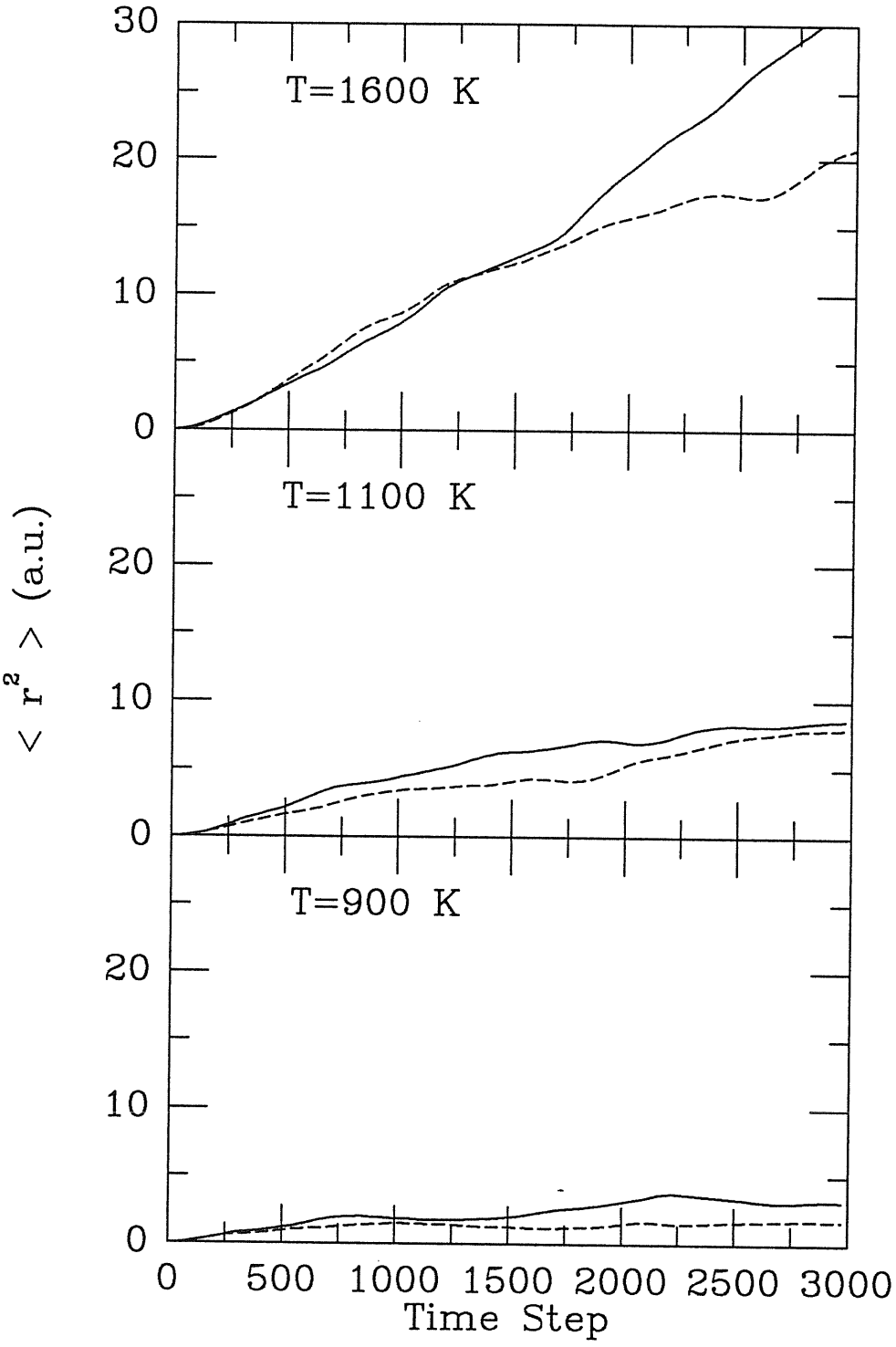

Figure 5.1: The mean square displacements of Ga (full line) and As (dashed line) atoms at three different temperatures.

this chapter refer to temperatures down to T=900 K, where a number of features of the amorphous phase seem already to be present.

The technical details of the simulation are almost the same as those used in chapter 4. We find however that the deviations from the BO surface decrease with decreasing temperature (the thickness of BO surface at T=900K is only ~20 K). This suggests that a gap is opening in the energy spectrum and thus a transition from a metallic to a semiconducting phase is taking place. The size of the MD cell is relaxed gradually to give the same density as in solid GaAs. The mass associated with the Nosè thermostats is adjusted with the temperature according to Eq.(A15). We decrease 100 K of temperature in 3000 time steps, giving a cooling rate $\sim 1 \times 10^{14}$ K/s, whereas the experimental quenching techniques can usually achieve only $\sim 10^{8}$ K/s[4].

The mean square displacements, $< r^2 >$, of Ga and As atoms in the system at three different temperatures (T=1600, 1100, 900 K) are shown in Fig. 5.1. In the upper panel the results for the liquid are shown for comparison. The behavior of $< r^2 >$ in the middle panel indicates the system is a supercooled liquid even at T=1100 K, while that in the lower panel shows a tendency to saturation, implying a sharp increase of viscosity and hence suggesting that freezing is undergoing in the system.

Fig.5.2 shows the BT partial structure factors at T=900K. The particle number structure factor $S_{NN}(k)$ of the liquid (see Fig.4.4) has a broad first peak which is here split into two sharper peaks. The arrows in Fig.5.2 give the position of the first two peaks in a X-ray study of a-GaAs at room temperature, which coincide with the first two peaks in c-GaAs[3]. The concentration structure factor $S_{CC}(k)$ has a more pro-

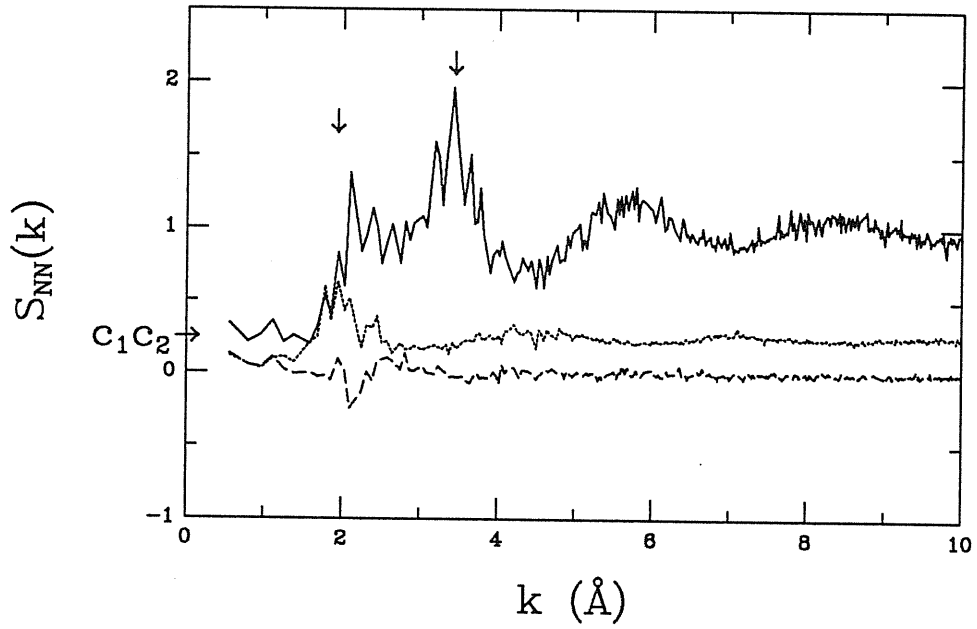

Figure 5.2:

The number-concentration (or BT) structure factors. The full line is S_{NN}, the dot line is S_{CC} and the dashed line gives the cross term S_{NC}. the two arrows denote the position of the first two peaks in X-ray diffraction results for a-GaAs[3].

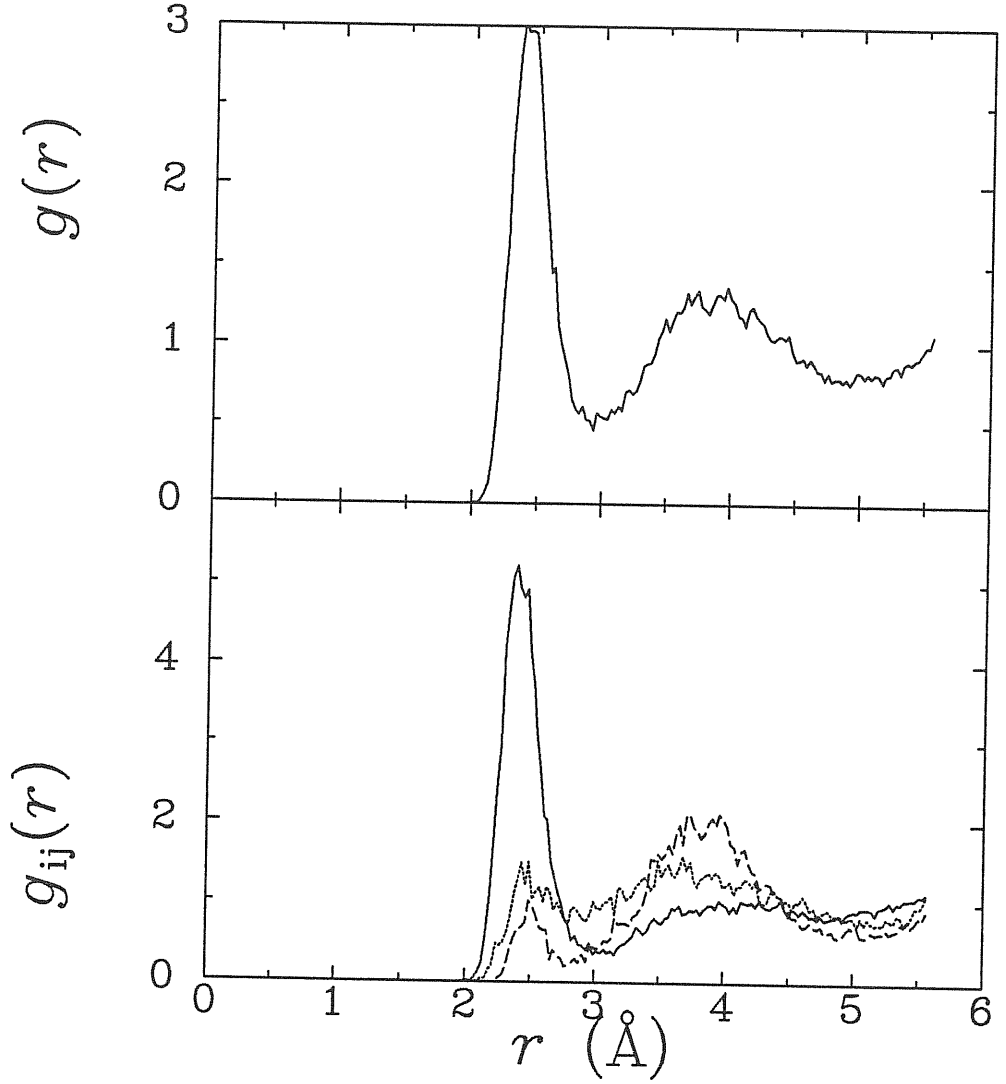

Figure 5.3: Upper panel: pair correlation function $g(r)$ of the system at T=900 K. Lower panel: $g_{GaAs}(r)$ (full line), $g_{GaGa}(r)$ (dot line) and $g_{AsAs}(r)$ (dashed line).

nounced peak than that in l-GaAs at $k \sim 1.95\AA^{-1}$, indicating a better

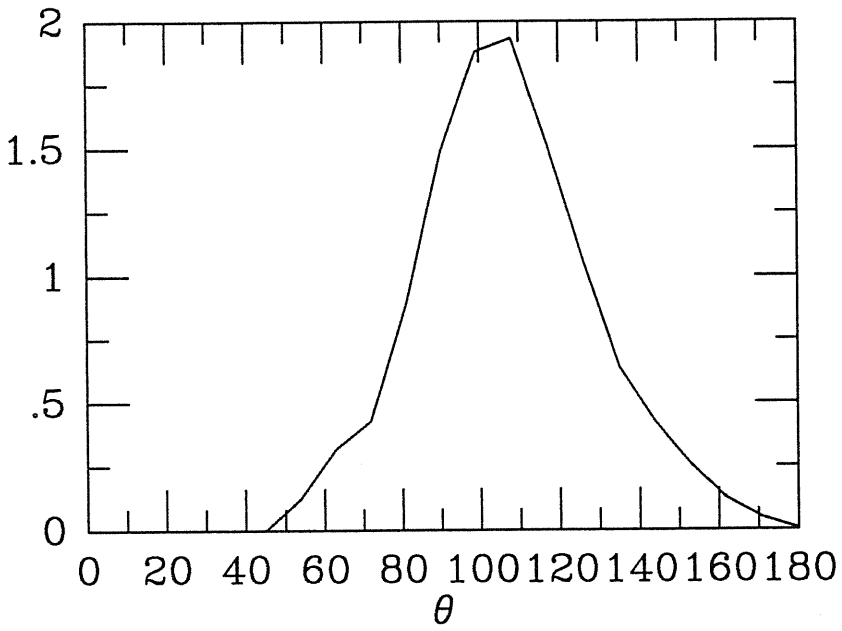

Figure 5.4: The bond angle distribution of the system at T=900 K.

chemical order at lower temperatures.

The pair correlation function is shown in Fig.5.3(a). The first peak is sharper than that in l-GaAs and the second which is almost absent in the liquid case has become quite prominent. The coordination number can be approximately estimated as 5.0 by integration of $4\pi\rho r^2 g(r)$ up to the first minimum at $r_{min} \sim 2.91\text{Å}$, to be compared with the value 6.3 in l-GaAs.

A dramatic change of the partial pair correlation functions can be seen in Fig.5.3(b), where it appears that the first peak of unlike-atom pairs has increased appreciably while that of like-atom pairs is reduced. This means that the nearest neighbour shell is dominated by unlike atoms. However "wrong bonds" still have an appreciable portion.

The bond angle distribution calculated using a cut-off distance $d_{cov} \sim 2.56\mathring{A}$ (see chapter 4) is shown in Fig. 5.4. A pronounced peak locates around $\theta \sim 109°$, suggesting that a tedrahedral structure is formed by reducing the temperature.

In summary, the results of this chapter suggest that an amorphous structure forming during the simulated quenching, although the temperature so far is as high as 900K.

Chapter 6

Conclusion

In this work, a first-principle molecular dynamics (Car-Parrinello) method is used to investigate the disordered phase of GaAs. This is the first time that this method is applied to a compound system. In this approach both atomic and electronic properties are obtained simultaneously.

Our results for the liquid phase of GaAs agree well with the limited experimental information available. A detailed picture of the local order is obtained as well. In agreement with experiments, we have found that this compound system has many similarities with l-Si and l-Ge[1]: a transition from semiconducting to metallic behavior occurs upon melting and the first-shell coordination number is increased at the same time. Although more atoms are found in this shell on average, it is observed that not all of them bond to the central atom. Each atom has $\sim$2.9 bonds on average, which is less than that in c-GaAs, and hence the portion of dangling bonds must be appreciable. In addition, we have found that the occurrence of "wrong bonds" between like-atoms is very frequent, while the formation of clusters of more than three atoms of a single species, is unlikely. These dangling bonds and "wrong bonds" should be

responsible for the dramatical increase of electrical conductivity upon melting.

A quenching process from liquid to amorphous GaAs is also simulated. The saturation of the atomic mean square displacements at the temperature around 900 K suggests a freezing in the system. The analysis of the bond angle distribution at this temperature indicates a prominent tetrahedral structure, revealing that amorphisation is taking place. However, an appreciable fraction of "wrong bonds" still exist at this temperature. A better amorphous structure is expected at room temperature.

As shown also by the previous studies on elemental systems, the Car-Parrinello method is an effective tool for the study of a variety of properties of disordered materials.

Appendix A

The Nosè Thermostat

In the standard classical molecular dynamics(MD) method, the newton's equations of motion for the particles (*e.g.* eq.(2.1)) are solved numerically. The total energy E is conserved, and thus the ensemble generated by the simulation is the microcanonical or (E, V, N) ensemble. The temperature in this ensemble is not constant, making it difficult to compare the simulation results with experiments.

To perform a MD simulation at constant temperature, one can simply keep the kinetic energy constant by periodically scaling the velocities of the ions. However, there seems to be no rigorous proof that this approach produces configurations belonging to the canonical ensemble.

A method to generate canonical ensemble averages via MD simulations was proposed by Nosè[30] a few years ago. He introduced an extra degree of freedom s in addition to the coordinates $\{\vec{R}_I\}$ of the N particles in a fixed volume V. The interaction between the physical system and s is expressed via the scaling of the velocities of the particles,

$$\vec{v}_I = s\dot{\vec{R}}_I \qquad (A1)$$

and $\vec{v}_I$ is considered as the real velocity of particle I. This can be interpreted as an exchange of heat between the physical system and the external system (thermostat).

The Lagrangian of Nosè's extended system is as

$$L = \sum_I \frac{M_I}{2} s^2 \dot{\vec{R}}_I^2 - \phi(\{\vec{R}_I\}) + \frac{Q}{2}\dot{s}^2 - (f+1)kT_{eq} \ln s \qquad (A2)$$

where M_I is the mass of the I-th particle, $\phi(\{\vec{R}_I\})$ is the potential of the physical system, the parameter Q can be thought as the fictitious mass associated with s, f is the number of degrees of freedom in the physical system, k is Boltzmann's constant and T_{eq} the externally set temperature value. The Lagrangian (A2) generates a dynamics for $\{\vec{R}_I\}$ and s through the equations of motion,

$$\ddot{\vec{R}}_I = -\frac{1}{M_I s^2}\nabla_{\vec{R}_I}\phi - \frac{2\dot{s}}{s}\dot{\vec{R}}_I \qquad (A3)$$

$$Q\ddot{s} = \sum_I M_I s \dot{\vec{R}}_I^2 - \frac{(f+1)kT_{eq}}{s}. \qquad (A4)$$

If we denote the average in the extended system by $< \cdots >$, the relation

$$< \frac{\sum_I M_I s^2 \dot{\vec{R}}_I^2}{s} >= (f+1)kT_{eq} < \frac{1}{s} > \qquad (A5)$$

is obtained from (A4), because the time average of a time derivative (*e.g.* $Q\ddot{s}$) vanishes. This suggests that the average of the kinetic energy coincides with the externally set temperature T_{eq}.

The hamiltonian

$$H_1 = \sum_I \frac{\vec{p}_I^2}{2M_I s^2} + \phi(\{\vec{R}_I\}) + \frac{p_s^2}{2Q} + (f+1)kT_{eq} \ln s \qquad (A6)$$

is a conserved quantity, where the momenta are given by

$$\vec{p}_I = \frac{\partial L}{\partial \dot{\vec{R}}_I} = M_I s^2 \dot{\vec{R}}_I \qquad (A7)$$

and

$$p_s = \frac{\partial L}{\partial \dot{s}} = Q\dot{s}. \qquad (A8)$$

Nosè proved that the equations of motion (A3) and (A4) produce configurations in the canonical ensemble at temperature T_{eq}. The argument is the following. The extended system produces a microcanonical ensemble of (f+1) degree of freedom. The partition function of this ensemble is defined by

$$Z = \frac{1}{N!}\int dp_s \int ds \int d\vec{p} \int d\vec{R}\delta(\sum_I \frac{\vec{p}_I^2}{2M_I s^2} + \phi(\vec{R}) + \frac{p_s^2}{2Q} + (f+1)kT_{eq}\ln s - E) \qquad (A9)$$

where the shortened form $d\vec{p} = d\vec{p_1}\cdots d\vec{p_N}, d\vec{R} = d\vec{R_1}\cdots d\vec{R_N}$ are used.

If we transform

$$\frac{\vec{p_I}}{s} = \vec{p_I'} \qquad (A10)$$

we obtain

$$Z = \frac{1}{N!}\int dp_s \int d\vec{p'} \int d\vec{R} \int ds s^f \delta(\sum_I \frac{\vec{p'}_I^2}{2M_I} + \phi(\vec{R}) + \frac{p_s^2}{2Q} + (f+1)kT_{eq}\ln s - E) \qquad (A11)$$

Using the equivalence relation for $\delta-$function $\delta(g(s)) = \delta(s - s_0)/g'(s)$, where s_0 is the value which makes $g(s_0) = 0$, and the shortened form

$$H(\vec{p'}, \vec{R}) = \sum_I \frac{\vec{p'}_I^2}{2M_I} + \phi(\vec{R})$$

we obtain

$$Z = \frac{1}{N!}\int dp_s \int d\vec{p'} \int d\vec{R} \int ds \frac{s^{f+1}}{(f+1)kT_{eq}}\delta(s - \exp[-\frac{H(\vec{p'}, \vec{R}) + p_s^2/2Q - E}{(f+1)kT_{eq}}])$$

$$\frac{1}{(f+1)kT_{eq}N!}\int dp_s \int d\vec{p'} \int d\vec{R} \exp[-(H(\vec{p'}, \vec{R}) + \frac{p_s^2}{2Q} - E)/kT_{eq}]$$

where

$$s_0 = \exp[-\frac{H + p_s^2/2Q - E}{(f+1)kT_{eq}}].$$

Carrying the integration with respect to p_s, we finally obtain

$$Z = \frac{1}{(f+1)}(\frac{2\pi Q}{kT_{eq}})^{1/2} \exp(E/kT_{eq}) Z_c \qquad (A12)$$

where Z_c is the partition function of the canonical ensemble

$$Z_c = \frac{1}{N!} \int d\vec{p'} \int d\vec{R} \ \exp[-H(\vec{p'}, \vec{R})/kT_{eq}]. \qquad (A13)$$

Hence Z only differs from Z_c by a constant factor. With the quasier-godic hypothesis which relates the time average along the trajectory to the ensemble average, the average of any static quantity expressed as function of $\{\vec{p}/s(=\vec{p'}), \vec{R}_I\}$ along the trajectory determined by (A3) and (A4), is exactly a canonical ensemble average, *i.e.*

$$\lim_{t_0 \to \infty} \frac{1}{t_0} \int_0^{t_0} A(\vec{p}/s, \vec{R}) \ dt =< A(\vec{p}/s, \vec{R}) >=< A(\vec{p'}, \vec{R}) >_c . \qquad A(14)$$

In principle, static quantities are independent of the value chosen for the parameter Q. However, in practice due to the finite number of time steps in the simulation, eq.(A14) is not always satisfied. Too small Q values may give decoupling of s from the physical system, whereas too large Q values lead to insufficient sampling of phase space. According to Nosè[30], Q can be chosen as

$$Q = \frac{2fkT_{eq}}{\omega^2 < s >^2} \qquad (A15)$$

where ω is of the order the second moment of the frequency spectrum of the velocity autocorrelation function of the physical system. With this choice, variable s has the same order of time scale of the physical system.

As pointed out by Nosè[42], it is easy to extend this method to multiple thermostats.

Bibliography

[1] V.M. Glazov, S.N. Chizhevskaya, and N.N. Glagoleva, in *Liquid semiconductors*, Plenum Press (1969).

[2] C. Bergman, C. Bichara, P. Chieux and J.P. Gaspard, Journal de Physique **C8**, 97 (1985).

[3] N.J. Shevchik, and W. Paul J. Non-Cryst. Solids **13**, 1(1973/74)

[4] see S.R. Elliott, in *Physics of amorphous materials* Lonngman, 1983

[5] R. Car and M. Parrinello, Phys. Rev. Lett. **55**, 2471 (1985).

[6] G. Galli, R.M. Martin, R. Car and M. Parrinello, to be published.

[7] I. Štich, R. Car and M. Parrinello, to be published.

[8] R. Car and M. Parrinello, Phys. Rev. Lett. **60**, 204 (1988).

[9] G. Galli, R.M. Martin, R. Car and M. Parrinello, Phys. Rev. Lett. **62**, 555 (1989).

[10] A. Rahman, Phys. Rev. **136**, A405(1964)

[11] see, for example, J. Hafner, *From Hamiltonians to Phase Diagrams*, Springer-Verlag Berlin Heidberg 1987.

[12] F.H. Stillinger, and T.A. Weber, Phys. Rev. **B31**, 5262(1985)

[13] E.R. Cowley, Phys. Rev. Lett. **60**, 2379(1988)

[14] P. Hohenberg, and W. Kohn, Phys. Rev. **136**, B864(1964)

[15] W. Kohn, and L.J. Sham, Phys. Rev. **140**, A1133(1965)

[16] M.T. Yin, and M.L. Cohen, Phys. Rev. **B26**, 5668(1982)

[17] see, for example, A. Messiah, *Quantum Mechanics* Vol.*II*, North-Holland, 1965

[18] R. Car, M. Parrinello, and W. Andreoni, in *Proceedings of the First NEC Symposium of Fundamental Approaches to New Material Phases*, ed. by S. Sugano and S. Ohnishi, Springer-Verlag, Berlin, 1987.

[19] M.P. Teter, M.C. Payne, D.C. Allen, *Solution of Schrödinger Equation for Large System* (preprint)

[20] I. Štich, R. Car, M. Parrinello, and S. Baroni, Phys. Rev. **B39**, 4997(1989)

[21] L. Verlet, Phys. Rev. **159**, 98(1967)

[22] R. Car, and M. Parrinello, to be published on J. Phys.: Condens. Matter

[23] For a review, see M.L.Cohen, and Heine, in *Solid State Physics*, ed. by H.E. Ehrenreich, F. Seitz, and D. Turnbull, vol.24, Academic Press, New York, 1970

[24] D.R.Hamann, M.Schluter, and C.Chiang, Phys. Rev. Lett. **43**, 1494(1979)

[25] J. Ihm, A. Zunger, and M.L. Cohen, J. Phys. C **12**, 4409(1979)

[26] L. Kleinman and D.M. Bylander, Phys. Rev. Lett. **48**, 1425 (1982).

[27] G.B. Bachelet, D.R. Hamman and M. Schluter, Phys. Rev. **B26**, 4199 (1982).

[28] see, G.B. Bachelet, and N.E. Christensen, Phys. Rev. B**31**, 879(1985) and references therein.

[29] R.C. Weast, in *Handbook of Chemistry and Physics*, 62nd ed., CRC, Boca Raton,1988.

[30] S. Nosè, Mol. Phys. **52**, 255(1984), and J. Chem. Phys. **81**, 511(1984)

[31] N.W. Ashcroft, and D.C. Langreth, Phys. Rev. **156**, 685 (1967).

[32] L. Koester, in *Neutron Physics*, Springer Tracts in Modern Physics vol. 80, ed. by G. Hohler, Springer-Verlag, Berlin, 1977.

[33] A.B. Bhatia, and D.E.Thornton, Phys. Rev. **B2**, 3004 (1970).

[34] Yoshio Waseda, in *The Structure of Non-Crystalline Materials* McGraw-Hill (1980), p16.

[35] Landolt-Bornstein: Numerical Data and Functional Relationships in Science and Technology, ed. by K.-H. Hellwege, vol.17, Springer-Verlag, Berlin (1984), p.341.

[36] X.-G. Gong, G. Chiarotti, M. Parrinello and E. Tosatti, to be published.

[37] L.F. Mattheiss, D.R. Hamann, and W. Weber, Phys. Rev. **B34**, 2190 (1986).

[38] R. Bellisent, C. Bergman, R. Ceolin, and J.P. Gaspard, Phys. Rev. Lett.**59**, 661 (1987).

[39] M.L. Cohen, and J.R.Chelikowsky, *Electronic Structure and Optical Properties of Semiconductors*, Springer-Verlag, Berlin, (1988), p109.

[40] see E.N. Economou, in *Green's functions in Quantum Physics*, Springer-Verlag, Berlin (1983), p152.

[41] see, for example, *Theory of Inhomogeneous Electron Gas*, eds. by S. Lundquist, and N.H. March, (Plenum, New York 1983) and references therein.

[42] S. Nosè, Mol. Phys. **57**, 187(1986)

[43] K.M. Shvarev, B.A. Baum, and P.V. Gel'd, Sov. Phys. Solid State **16**, 2111 (1975).

[44] I. Štich, Ph. D thesis, International School for Advanced Studies,Trieste, 1989.